

This work is on a Creative Commons Attribution 4.0 International (CC BY 4.0) license, <https://creativecommons.org/licenses/by/4.0/>. Access to this work was provided by the University of Maryland, Baltimore County (UMBC) ScholarWorks@UMBC digital repository on the Maryland Shared Open Access (MD-SOAR) platform.

Please provide feedback

Please support the ScholarWorks@UMBC repository by emailing [scholarworks-group@umbc.edu](mailto:scholarworks-group@umbc.edu) and telling us what having access to this work means to you and why it's important to you. Thank you.

## REVIEW

# Emerging theranostic applications of carbon dots and its variants

Priyanka Ray<sup>1,3,†</sup> | Parikshit Moitra<sup>1,2,†</sup> | Dipanjan Pan<sup>1,2,3</sup> 

<sup>1</sup> Department of Chemical, Biochemical, and Environmental Engineering, University of Maryland Baltimore County, Baltimore, Maryland, USA

<sup>2</sup> Department of Pediatrics, Center for Blood Oxygen Transport and Hemostasis, University of Maryland Baltimore School of Medicine, Baltimore, Maryland, USA

<sup>3</sup> Department of Diagnostic Radiology and Nuclear Medicine, University of Maryland Baltimore, Baltimore, Maryland, USA

## Correspondence

Dipanjan Pan, Department of Chemical, Biochemical, and Environmental Engineering, University of Maryland Baltimore County, Baltimore, MD 21250, USA.  
Email: [dipanjan@som.umaryland.edu](mailto:dipanjan@som.umaryland.edu)

<sup>†</sup>Equal contribution

## Funding information

University of Maryland Baltimore, University of Maryland Baltimore County

## Abstract

In recent years, carbon dots (CDs), that is, carbon nanoparticles less than 10 nm in size with unique molecular properties including photoluminescence, biocompatibility, and water dispersibility, have been widely used in various fields of nanobiotechnology. This review article aims to describe the recent progress on CD research with a focus on their chemical composition and varieties as well as a comparative section on graphene quantum dots. The following sections shed light on the synthetic routes towards the fabrication of CDs followed by an elaborate description of their emerging applications in theranostics. Finally, a perspective is provided to indicate the major roadblocks for the translation of CDs from research laboratories to the clinics. This article thus aims to update the latest results in this rapidly developing field and offers crucial insights to inspire novel and exciting research in this domain.

## KEYWORDS

carbon dots, diagnostics, drug delivery, imaging, theranostics

## 1 | INTRODUCTION

Nanotechnology is a blooming area of research garnering increasing interest in academia and clinics with the passage of time. In this regard, the use of nanoparticles, especially quantum dots (QDs) have emerged as popular candidates due to their unique quantum confinement properties. Despite possessing numerous advantageous properties, inorganic semiconducting QD materials still face major drawbacks in terms of their application in

the clinical arena primarily due to their biocompatibility issues.<sup>1,2</sup> Scientists were therefore in constant pursuit of an alternative and the emergence of carbon dots (CDs) as a novel class of luminescent nanomaterials has revolutionized the field of nanoparticle research. CDs, primarily classified as carbon nanodot, carbon quantum dot (CQD), carbonized polymer dot (CPD), and graphene quantum dot (GQD),<sup>3,4</sup> displayed their superior properties as compared to the traditional organic fluorescent dyes and inorganic semiconductor quantum dots. The advantages of CDs include but are not limited to their facile preparation and purification techniques, tunable photoluminescence (PL) emission, availability of surface functional groups, superior photostability, and excellent biocompatibility.<sup>5</sup> Subsequently, CDs are explored in many different

**Abbreviations:** CD, carbon dot; CQD, carbon quantum dot; CPD, carbonized polymer dot; ECL, electrochemiluminescence; GPD, graphene quantum dot; HOMO, highest occupied molecular orbital; NP, nanoparticle; PL, photoluminescence; PV, photovoltaic; QD, quantum dot; QY, quantum yield.

This is an open access article under the terms of the [Creative Commons Attribution](https://creativecommons.org/licenses/by/4.0/) License, which permits use, distribution and reproduction in any medium, provided the original work is properly cited.

© 2021 The Authors. *VIEW* published by Shanghai Fuji Technology Consulting Co., Ltd, authorized by Professional Community of Experimental Medicine, National Association of Health Industry and Enterprise Management (PCEM) and John Wiley & Sons Australia, Ltd.

applications including bioimaging, sensing, optoelectronic devices, drug delivery, catalysis, anti-counterfeiting, etc., where CDs have been demonstrated as an emergent frontier nanomaterial. The afterglow CD materials<sup>6</sup> with longer shelf-life, improved phosphorescence, and delayed fluorescence also deserve special emphasis in this regard. Thus, in lieu of their scientific significance and advanced applications, numerous review articles have been published to date on CDs summarizing the various aspects of their synthetic methods, unique photophysical properties, and potential applications in different fields, for example, theranostics, industry, and agriculture. However, it is very important to be up to date in the rapidly evolving field of CD research, and we believe that this review will address to this need.

In this review article, we initially provide a brief introduction to the chemical composition and types of CDs (Section 2). A special emphasis has been given on graphene and CQDs, CDs with dopants, and amorphous CDs with a discussion on structural differences among different carbon nanoparticle variants. The important synthetic routes, for example, microwave irradiation, hydrothermal, solvothermal, laser ablation, ultrasonication, ball milling, and electrochemical processes among others are then elaborated for the preparation of CDs with superior photochemical properties (Section 3). Some potential applications of CDs especially in the areas of bioimaging, diagnostics, electroluminescence, drug delivery, etc. are then discussed (Section 4). These aspects of carbon dots are schematically represented in Figure 1. Finally, challenges regarding the employment of CDs and certain perspectives in terms of their design strategies, properties, and application opportunities are provided (Section 5 and 6), which may pave their translation from the laboratory to the commercial arena.

## 2 | CHEMICAL COMPOSITION AND TYPES OF CDs

Despite a lot of debates on the definition and classification of CDs, a general definition stems from a broad range carbon-based luminescent nanomaterials, doped with heteroatoms like oxygen, nitrogen, sulfur, etc., with sizes less than 10 nm. CDs are primarily divided into three categories depending upon their morphologies and chemical structures. These are GQDs, CQDs, and CPDs. As evident from the names, GQDs are generally composed of nanosized graphene with perfect sp<sup>2</sup> carbon structure,<sup>7</sup> CQDs are composed of almost complete sp<sup>2</sup> cores, whereas CPDs are made up of amorphous CDs with defined polymer shell.<sup>5</sup> Most of the CDs show strong UV absorption with a tail extending in the visible region,

where the peaks may be assigned to the  $\pi$ - $\pi^*$  (C=C bond) or n- $\pi^*$  transition (C=O bond). Notably, all these CD variants have definite functional groups on their surfaces (amino, hydroxyl, carboxyl, etc.) which led to their water solubility and user-defined control. The user-defined control allows the user to control the size and shape as well as aggregation properties of the nanoparticles for their application in diverse fields of nanobiotechnology.<sup>1,8</sup>

### 2.1 | Graphene and carbon quantum dots

CQDs, often called carbon dots,<sup>9</sup> are fluorescent carbon nanoparticles with size < 10 nm, high chemical stability, good conductivity, high luminescence, and broadband optical absorption.<sup>10</sup> GQDs are usually a subset of CQDs made of graphene and/or graphene oxide.<sup>11</sup> If composed of <10 graphene layers, GQDs generally are <10 nm in the lateral dimension. In such a case, GQDs exhibit physicochemical properties similar to graphene.<sup>12</sup> However, some properties of GQDs are unique due to the dominance of edge effects and quantum confinement.<sup>13</sup> The increased PL of CQDs generally originate from different mechanisms, including photoexcitons of carbon, size effect, surface groups, emissive traps, aromatic structures, edge defects, and free zigzag sites. Researchers had also studied the origin of CD PL with subsingle-particle resolution and related the mechanism to sp<sup>2</sup> domain size and copious presence of oxidized surface defects. With the help of single-molecule absorption scanning tunneling microscopy (SMA-STM),<sup>14</sup> it has been demonstrated that with increasing number of oxygen-containing defects, the PL of CDs can be shifted from blue to green to yellow and red emission (Figure 2). Imaging of density of states revealed that graphitic core has a large bandgap which is reduced to smaller gaps by localized defects generating both red-emitting dots (rCDs) and blue-emitting dots (bCDs). Several reports indicated that solvothermal CDs are composed of surface-accessible spatially localized oxidized defects, most likely carboxylates and phenolic hydroxyls.<sup>14,15</sup> These functional groups are responsible for their fluorescence properties. While models for fluorescence redshift in solvothermally prepared CDs based on degrees of sp<sup>2</sup>-hybridization of carbon surface domains exist, recently reported results using SMA-STM suggest that emission from oxygen-rich surface defects is the major mechanism due to direct imaging of localized optically active defects and the sensitivity to pH of the CDs (Figure 2). An increase in these defects results in red fluorescence, which is indicative of an increase in a probability of defects with smaller energy gaps. However, SMA-STM revealed that the emissive defects do not always have the smallest electronic bandgap, which is associated with the emission wavelength.<sup>15</sup>

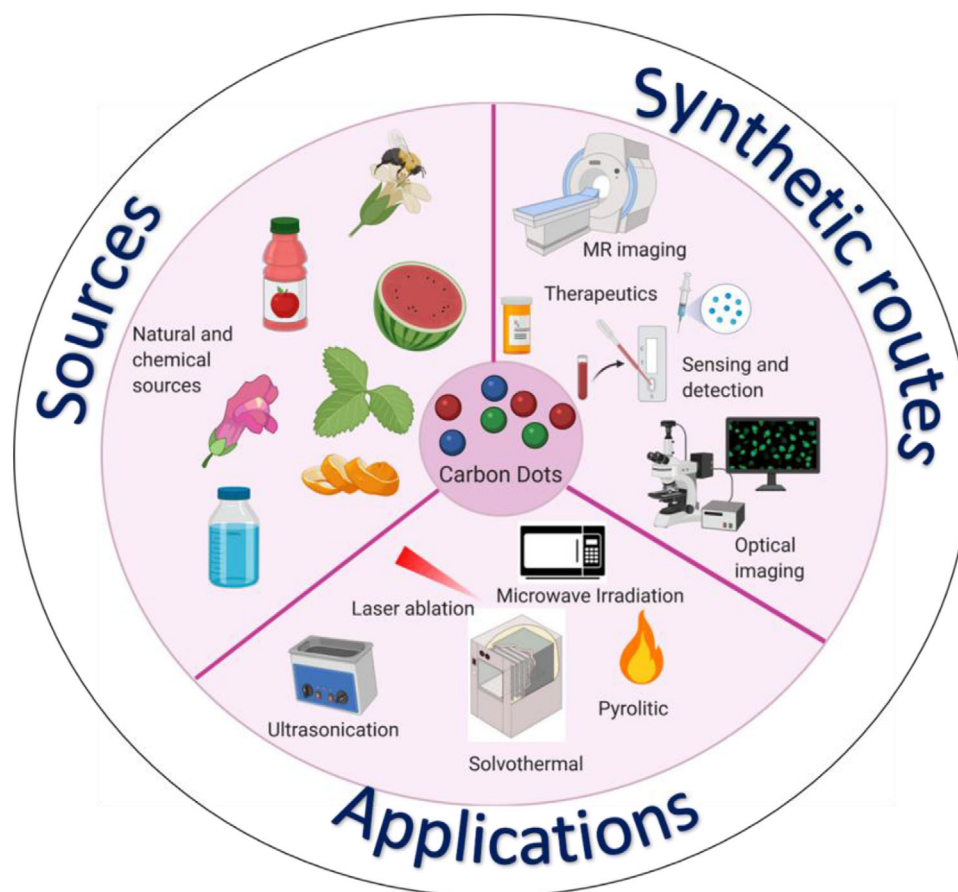


**FIGURE 1** Schematic representation of some sources and methods used for the synthesis of CDs and their applications in the biomedical field.

GQDs are often synthesized from graphene-like polycyclic aromatic hydrocarbon molecules<sup>16</sup> and hence exhibit higher crystallinity and less defects owing to the presence of an increased number of crystalline sp<sup>2</sup> carbon. Consequently, both GQDs and CQDs generally possess lattice structure similar to single or a few layered graphene crystalline structure where the in-plane lattice spacing range from 0.18 to 0.25 nm.<sup>17</sup> Importantly, CQDs have an abundance of oxygen-containing functional groups including carbonyl, hydroxyl, carboxylic acid, epoxy/ether on their surfaces in contrast to their starting materials. Also, in comparison to the inorganic semiconducting quantum dots, for example, CdS, CdSe quantum dots, CQDs demonstrate superior photostability and potentially lower cytotoxicity which can be attributed to the presence of large amount of surface carboxyl moieties. Researchers have largely exploited these surface functional groups available for CQDs to alter their biochemical properties.<sup>18,19</sup> Chemical modification of GQDs with strong electron-accepting and electron-donating molecules also modified their electronic properties<sup>20</sup> either by decreasing the lowest unoccupied molecular orbital levels or by raising the highest occupied molecular

orbital (HOMO) levels, respectively. In this regard, Zhu et al.<sup>21</sup> successfully modified green fluorescent GQDs into blue luminescent GQDs simply by altering the surface functionalities with alkylamines (Figure 3). These chemical modifications decreased the nonradiative recombination and converted the GQDs from a defect state to an intrinsic emissive state. Zhang et al.<sup>22</sup> found GQDs when reduced with hydrazine hydrate demonstrated a strong yellow luminescence which changed to weak blue fluorescence when reduced with sodium borohydride. It was hypothesized that the introduction of hydrazide groups to the edges of GQDs led to the  $\pi$ - $\pi^*$  and  $n$ - $\pi^*$  transitions and resulted in the strong yellow luminescence. Interestingly, the reduced CDs can further be reoxidized to regain the original fluorescence, and the oxidation–reduction cycle can be repeated.<sup>23</sup> Surface chemistry thus played a critical role in exhibiting the absorption and emissive behavior of CDs. CDs prepared from a solvothermal synthetic process in the presence of an alkali (NaOH or KOH) exhibited orange emission with quantum yield as high as 46%.<sup>24</sup> However, the quantum yield dropped to 6% when the surface coordinated metal cations were removed with dilute aqueous HCl solution generating an



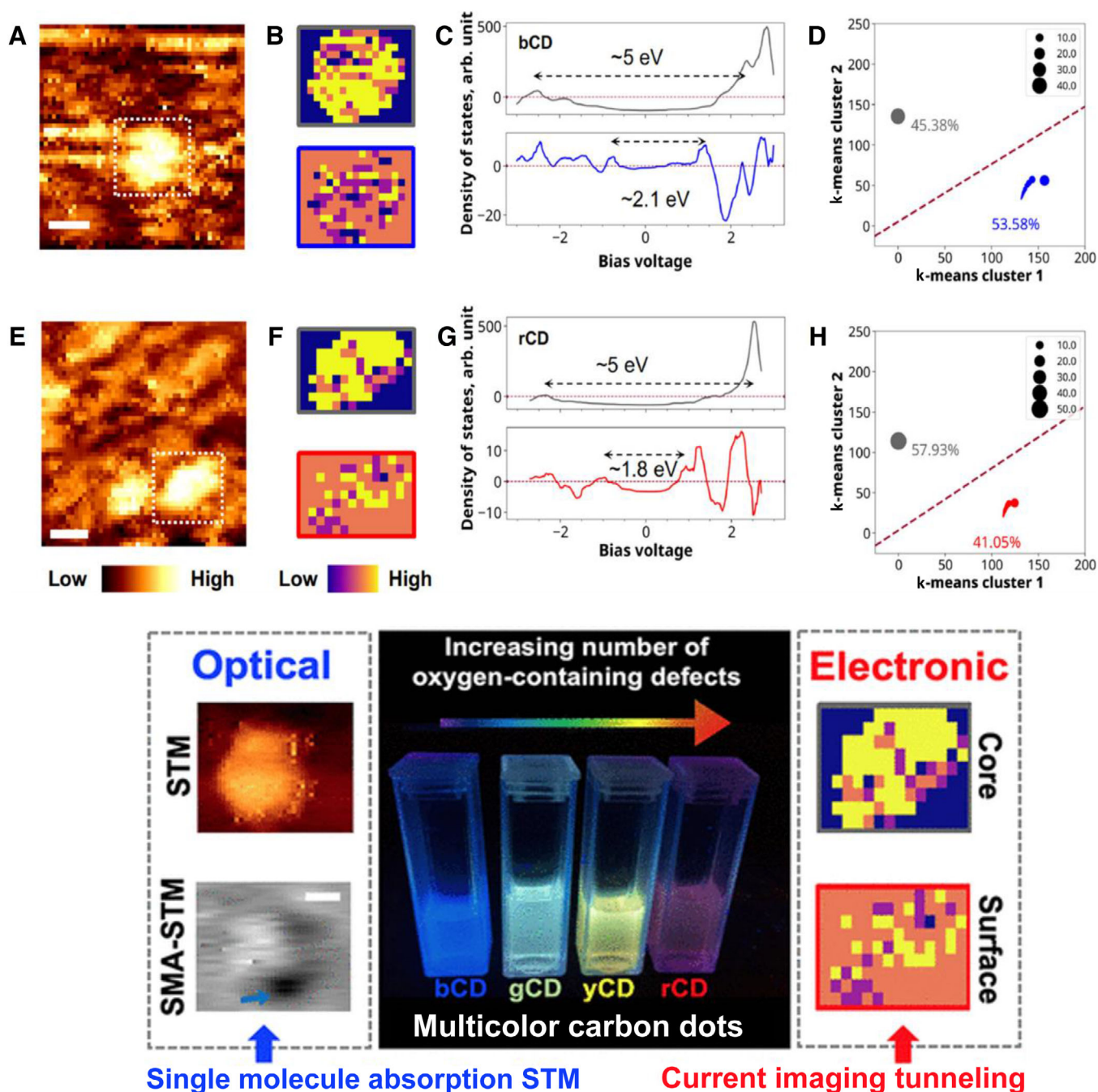


**FIGURE 2** Understanding the relation between the PL of carbon dots with oxygen-containing defects.<sup>14</sup> Density of states imaging of blue- and red-emitting carbon dots. (A, E) Topographic images of (A) one bCD and (E) one rCD in a dashed white box with scale bars of 5 nm and colormap indicating STM height. (B, F) Two groups of spatial components resulting from PCA and *k*-means clustering of the CITS data for the CDs in panels A and E; the gray frame indicates image for PCA component 1 group and the (B) blue- and (F) orange-colored frames indicate the PCA component 2 group; the colormap indicates low (blue) to the high (yellow) density of states, showing that PCA1 covers the core of the CD, whereas PCA 2 consists of localized defects of about 1–2 nm in diameter. (C, G) Weighted averaged density of state spectra of the PCA groups 1 and 2, core (gray) and defect (blue/red). The dashed double-sided arrows indicate the observed electronic bandgaps for these two groups of features. (D, H) Two groups of PCA components for bCDs and rCDs (color coded), respectively, separated by *k*-means clustering. The dashed line represents the decision boundary. A graphical representation of the comparison of optical and single-molecule absorption STM results for multicolor carbon dots. (Reprinted with permission from Ref. 14)

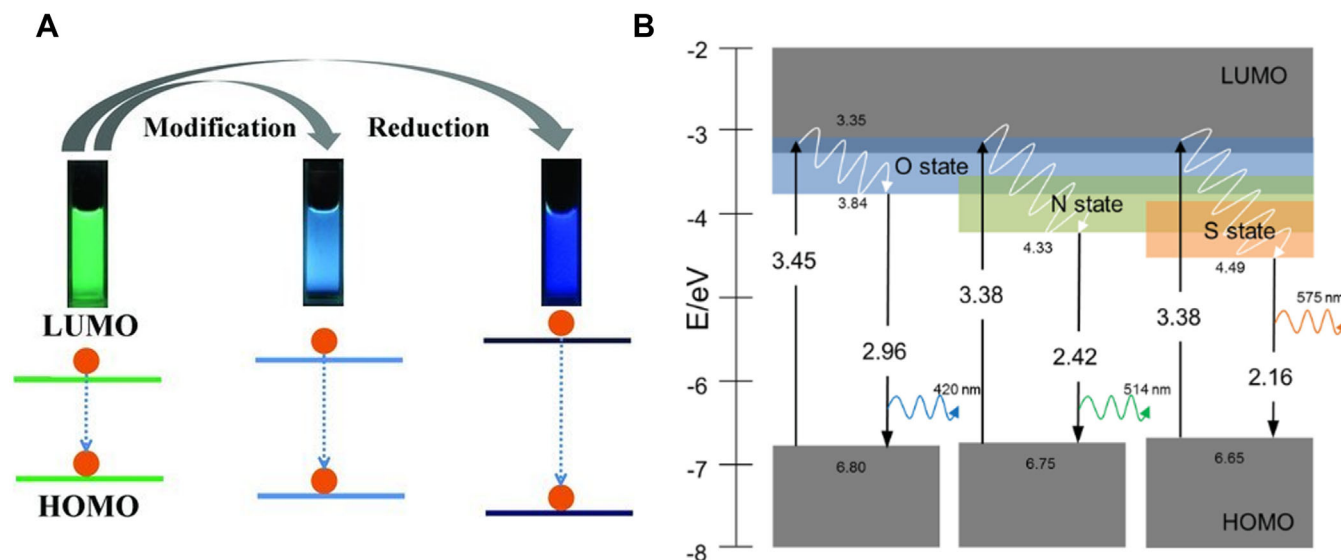


**FIGURE 3** (A) Schematic representation of change in the bandgap of GQDs.<sup>21</sup> (B) Change in the bandgap of CDs with doping of N and S (reprinted with permission from Refs. 21 and 27)

increased overlap between the absorption and emission spectra. Therefore, the generation of increased quantum yield can be attributed to the presence of surface metal-cation-functionalization that could lift the Fermi level of CDs and demonstrate reduced self-absorption and enhanced emission. In another study, results showed that the oxidizable surface abundant functionalities on CD are prone to aerial oxidation and with an increase in aerial oxidation, a remarkable shift in the emission peak was observed.<sup>25</sup> This could be attributed to the gradual decrease in their respective band gaps leading to the redshift in fluorescence emission. A comparative study of bulk- and single-particle properties was performed to understand the photophysical properties of CDs as a function of precursor composition and reaction temperature.<sup>26</sup> This study revealed the formation of particles with smaller diameters and high quantum yield with a narrow emission band when synthesized at a temperature of 200°C. However, the same process when carried out at 150°C, formed nanoparticles (NPs) presented increased colloidal and photostability with a redshift in their fluorescence emission and greater UV-visible absorbance. The data indicate the important role of temperature to control the photophysical properties of CDs.

Similarly, CQDs conjugated with polyamidoamine (PAMAM) and (3-aminopropyl)triethoxysilane (APTES) exhibited higher fluorescence compared to CQDs conjugated with PAMAM or APTES alone. This was due to the presence of multiple oxygenated and nitrous groups on the surface of the CQDs,<sup>28</sup> facilitating a high yield of radiative recombination and hence increased PL. On the other hand, GQDs functionalized with primary amine (NH<sub>2</sub>-GQDs)

and dimethylamine (NMe<sub>2</sub>-GQDs) had degenerate HOMO orbitals and higher energy levels, whereas GQDs modified with azo (Azo-GQDs), *o*-phenylenediamine (OPD-GQDs), *p*-methyl red (pMR-GQDs), and diaminonaphthalene (DANGQDs) had lower energy levels.<sup>29</sup> Further, the surface modification of CQDs to introduce tunable amphiphilicity largely impacted their fluorescence and physical properties and resulted in their transfer between oil and water phases. In this context, positively charged CQDs capped with imidazolium-based ionic liquid, using citric acid as a carbon source were also prepared. Following this, the amphiphilicity of the as-prepared CQDs was tuned by anion exchange methodology. There are also multiple reports where CQDs were used in developing unique composite and hybrid materials.<sup>30</sup> Their surface functionalities played an important role in this direction by tuning their properties for therapeutic and diagnostic purposes. It was observed that when functionalized with thiourea GQDs completely lost their ability to produce singlet oxygen (<sup>1</sup>O<sub>2</sub>) upon photoexcitation and hence could be used as efficient •OH quenchers. On the other hand, GQDs functionalized with urea improved their capability to produce <sup>1</sup>O<sub>2</sub> upon the same conditions and could be used as an efficient photosensitizer.<sup>31</sup> Thus, GQDs and CQDs, in general, owe interesting PL properties due to their excitation wavelength-dependent emission, excellent biocompatibility, enhanced photostability, and improved chemical inertness.<sup>32</sup> While GQDs are typically derived from graphene/graphite or different graphitic three-dimensional (3D) materials by top-down synthetic approaches, CQDs are generally synthesized by bottom-up preparation strategies. Separately, when

GQDs primarily exist in few-layer structures, with lateral dimension up to 100 nm, CQDs have spherical shape up to 10 nm.<sup>33</sup>

Nanocomposites such as a mixture of biodegradable chitosan and magnetic GQDs were used as microneedle arrays for the release of therapeutics; imprinted polymers on carbon nitride nanotubes/GQDs/core-shell nanoparticles were utilized for the electrochemical detection of phenylethanolamine A in human urine samples<sup>34</sup>; mixture GQDs and molecularly imprinted polymers (MIPs) were used for the electrochemical sensing of metronidazole and serotonin<sup>35</sup>; GQDS/MIPs coated on hollow nickel nanospheres for the electrochemical sensing of bisphenol S.<sup>36</sup> Further, MIP-coated CQDs demonstrated their extraordinary biocompatibility towards the targeting of cancer cells.<sup>37</sup> The doxorubicin-loaded zeolitic imidazolate framework with GQDs also showed their efficacy in killing cancer cells mediated by the combinatorial effect of chemotherapy and photothermal therapy.<sup>38</sup>

## 2.2 | CDs with dopants

It was understood that both the surface functionality and heteroatom doping can influence the molecular properties of CQDs. Especially, doping can influence the electronic and optical properties and surface reactivity of CQDs.<sup>39</sup> Among all, nitrogen doping is the most commonly employed strategy for generating N-doped CQDs towards the enhancement of CQDs' emission while inducing an upward shift in the Fermi level and electrons in the conduction band.<sup>40</sup> Qu et al. showed that the green luminescent GQDs can be modulated to generate blue luminescent N-doped GQDs with the introduction of tetrabutylammonium perchlorate in a solution of GQDs in acetonitrile.<sup>41</sup> This can be attributed to the stronger electron-withdrawing ability of the nitrogen atoms when introduced in the GQD assembly. A large increase in PL quantum yield was also found while introducing urea as the N-containing bases during the preparation of GQDs.<sup>42</sup> Nitrogen-doped CQDs were also prepared in a single step via the ultrasonic treatment of dopamine in dimethylformamide solution which exhibited better water solubility, lower photobleaching, pH-insensitive bright, and stable fluorescence, and improved biocompatibility.<sup>43,44</sup> Boron-doped CQDs, obtained through the one-pot solvothermal process also demonstrated higher longitudinal relaxivity and redshifted increased fluorescence intensity. The boron atom provides an empty orbital to the carbon p-system thus providing a reduction in the electron density level in the HOMO of CDs. This is contrary to the N-doped CDs, where nitrogen contributes a pair of electrons to the occupied p

orbitals, leading to the stabilization of HOMO level and a wider bandgap. Studies also demonstrated that a difference in nitrogen doping types and positions leads to the generation of different absorption and emission properties.<sup>45</sup> It was understood that while edge doping increases photoluminescent intensity by increasing the photoexcited electrons in the emission transition channel, center doping decreases the fluorescence emission intensity by creating nonluminescent midstates that block transition channels. Ye et al. studied the effect of doping electron-withdrawing fluorine atoms into CDs that demonstrated a red-shifted PL emission.<sup>46</sup> It was understood that CDs with edge-bearing oxygen species are p-type materials as oxygen is more electronegative in character than carbon atoms. Therefore, nitrogen doping in CDs repaired the vacancy-type defects and introduced n-type conductivity in CDs.<sup>47</sup> Overall, it is generally accepted that N doping can enhance the PL of CDs.<sup>27</sup> The electron transport properties, PL wavelength can also be tailored efficiently by N doping as most of the precursors used during the bottom-up synthesis are nitrogenous. N doping might therefore be more preferred due to its matched size with the carbon atom and N-type structure.<sup>48</sup>

The influence of both electron acceptor and electron donor on the photophysical properties of CDs were also investigated at the bulk-state and single-particle levels.<sup>49</sup> Lanthanides, for example, yttrium, were also doped in CDs to examine their influence on the photoluminescent properties and used for sensitive label-free detection of various pathogens at the single-cell resolution level.<sup>50</sup> A Mg/N codoping strategy was also developed to generate highly luminescent CQDs with a quantum yield of ~83%.<sup>51</sup> Similarly, P/N codoped CQDs were prepared via microwave irradiation of dimethylformamide in the presence of phosphoric acid,<sup>52</sup> while S/N codoped CQDs were synthesized while carbonizing hair fiber with sulfuric acid.<sup>53</sup> It was also demonstrated that higher temperature could lead to the formation of S/N codoped CQDs with smaller size, higher S content, a longer photoluminescent wavelength which showed enhanced PL stability, minimal toxicity, improved water solubility, and higher biocompatibility.

## 2.3 | Biocompatibility of CDs

Due to the structural composition of carbon dots and their variants, they are found to be highly biocompatible in nature. Even at a concentration much higher than required for imaging purposes, CDs do not present any significant cellular toxicity. CDs showed >90% cellular viability when tested against human hepatocellular carcinoma cells.<sup>54</sup> Ajayan et al. have shown that GQDs do not exhibit any



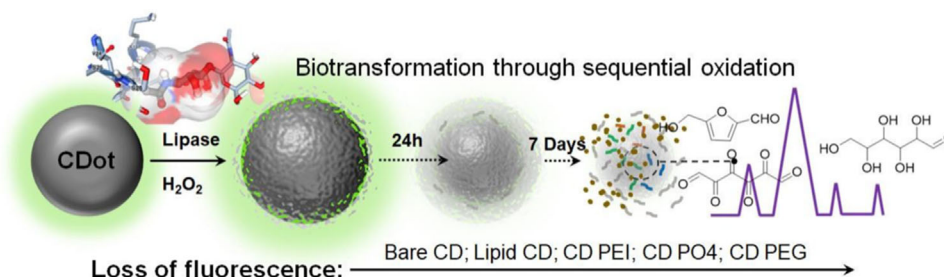


**FIGURE 4** Schematic representation of the biodegradation of carbon dots leading to the formation of hydroxymethylfurfural through sequential oxidation.<sup>62</sup> (Reprinted with permission from Ref. 62)

significant toxicity to human breast cancer cells even up to a dose of 50  $\mu\text{g/mL}$ .<sup>55</sup> The biocompatibility of GQDs was also evaluated in stem cells,<sup>22</sup> which require more stringent growth conditions, neurosphere cells, and cardiac progenitor cells at a concentration of 100  $\mu\text{g/mL}$  with an incubation period of 3 days, and pancreatic progenitor cells. Another study showed that GQDs, even at a concentration of 250  $\mu\text{g/mL}$ , showed minimal cellular toxicity. Insignificant changes in metabolic activity, self-renewal ability, and differentiation potential of human neural stem cells were also observed.<sup>56</sup> Scientists therefore successfully used macromolecularly “caged” carbon nanoparticles for intracellular trafficking purposes.<sup>57</sup>

Further, the hemolysis percentage was found to be <1.8% for a CD concentration of 60  $\mu\text{g/mL}$ .<sup>58</sup> By ISO guidelines, <5% is considered to be nonhemolytic. Further, in vivo toxicity of CDs was also evaluated in mice. Forty milligrams of polyethylene glycol (PEG) 1500N passivated CDs was injected intravenously into the mice which showed no change in their daily activities, food intake, body weight, kidney and liver functions, and alterations in serum biochemical indicators.<sup>59</sup> Inspired by this, the in vivo fate of CDs was also tested in mice through three different injection routes utilizing near-infrared fluorescence and positron emission tomography imaging.<sup>60</sup> Efficient and rapid clearance of CDs was found with the excretion rate ranked as intravenous > intramuscular > subcutaneous. It was also observed that CDs had comparatively low retention time in the reticuloendothelial system. Moreover, CDs demonstrated improved tumor-to-background contrast. A long-term distribution profile of PEG-functionalized GQDs showed minimal toxicity to the mice even at a dose of 20 mg/kg over a period of over 3 months. The PEG-coated GQDs primarily accumulated in the liver and spleen and then cleared with quick succession of time.<sup>61</sup> Studies showed that CDs undergo peroxide-catalyzed degradation in the presence of lipase and generated hydroxymethylfurfural as a metabolic by-product of the CDs<sup>62</sup> (Figure 4). Further, it was understood that differently charged CD species have different degradation kinetics when subjected to enzyme oxidation in a biolog-

ical environment exhibiting their diverse metabolic fate. All these experiments suggest the greater potential of CDs towards their application in the versatile field of theranostics. It must be kept in mind that before their translation for use in humans, the experiment evaluating the median lethal dose (LD<sub>50</sub>) of CDs should be performed. In addition, one must be careful about the synthetic strategies of CDs, as their cellular toxicity and hence biocompatibility largely depends on their preparation methodologies.

### 3 | SYNTHETIC ROUTES FOR CDs

The synthetic methods for CDs are broadly divided into the “top-down” and “bottoms-up” approach. The “top-down” approach involves the breakdown of bulk material into larger fragments employing a variety of techniques including arc discharge, laser ablation, ball milling, and electrochemical processes.<sup>63</sup> On the other hand, the “bottoms-up” method involves the use of smaller precursors using microwave synthesis,<sup>64</sup> ultrasonication,<sup>65</sup> acidic oxidation,<sup>66</sup> and green synthesis.<sup>67</sup> This section describes some of the widely employed processes for the formation of carbon dots, their advantages, and their pitfalls.

#### 3.1 | Laser ablation process

This process uses a high-energy laser pulse to generate high temperature and pressure by irradiating the surface of the target material.<sup>68</sup> Usually the carbon precursor dissolved in a solvent is placed in a glass cell in the presence of water vapor under an inert gas under high temperature and pressure is irradiated with a laser beam. The laser employed is a, Nd: YAG pulsed laser with a second harmonic wavelength of  $\sim 530$  nm.<sup>69</sup> Many groups have reported the preparation of fluorescent carbon dots by irradiating an organic precursor using this method,<sup>70,71</sup> followed by dissolution of the prepared particles in various organic solvents.<sup>72</sup> Such particles can be used for various imaging applications due to their wide range of



PL properties, which can be further modified by changing their surface properties.<sup>70</sup> However, this process has limited use to due lower cost-effectiveness and the used of skilled operators although it is a fast and green method of fabrication of CDs.

### 3.2 | Electrochemical process

This method uses electrochemical carbonization of organic sources with the application of direct electric current. organic compounds like alcohols undergo electrochemical carbonization reaction under basic conditions. The basic setup includes a three-electrode system with two Pt sheets as the working and counterelectrodes, as well as a calomel electrode mounted on a freely adjustable Luggin capillary acted as the reference electrode. The precursor solution is prepared by mixing alcohol with water in the ratio 14:1 in an alkaline solution. The current can be varied between 15 and 100 mA depending on the source of the C used. The process typically takes about 4 h at the end of which the transparent color of the solution changes to black or dark brown.<sup>69</sup> Following the completion of the reaction, the reaction mixture is salted out by adding ethanol and left to stand overnight. Solvent removal gives a solid residue which is further purified using dialysis against aqueous solutions using a suitable membrane with an optimal molecular weight cutoff.

This process has gained popularity due to its ease of use, controlled size formation, and efficiency. It is a type of top-down method which involves the oxidation of small organic molecules via electrochemistry. Various sources have been used as precursors for CDs including alcohols,<sup>73</sup> citrates,<sup>74</sup> and multiwalled carbon nanotubes.<sup>17</sup> Electrochemical oxidation has been reported to produce CDs with a high yield, purity, and to be cost-effective. The average diameter of particles thus produced is usually <5 nm although the applied electric potential is an important parameter for controlling the size of CDs.<sup>73</sup>

### 3.3 | Ball-milling process

Ball milling has been described as a green method to produce CDs and doped CNPs (carbon nanoparticles).<sup>75</sup> This is a solid-state type process eliminating the use of toxic solvents. solid-state processes.<sup>76</sup> This method uses energy to break down larger materials by using moving balls and harnessing their kinetic energy to break chemical bonds and create surfaces and structures which are exploited for various applications including catalysis. Usually, this process can generate high temperature<sup>77</sup> and pressure.<sup>78</sup>

### 3.4 | Ultrasonication

Ultrasonic treatment is an approach common to both bottom-up and top-down approaches to prepare CDs. While the top-down approach is achieved by using ultrasonic waves to break down large C-containing precursors, the bottom-up method has been reported to use acid-treated glucose<sup>65</sup> or peroxide-treated activated carbon<sup>79</sup> to produce CDs. These particles are reported to be monodisperse and homogeneous with a modifiable surface.<sup>80</sup> Various doped CDs have been produced using this method.<sup>81</sup> This method is popular due to its versatility, cost-effectiveness, and facile experimental procedure.

### 3.5 | Microwave irradiation

This is a widely used method for the preparation of carbon dots involving the heating of a small molecule, for example, glucose,<sup>65</sup> citrate,<sup>82</sup> xylose,<sup>83</sup> various organic sources including orange juice,<sup>84</sup> honey<sup>67, 85</sup> and caffeine in a controlled atmosphere for a specified time period. Usually a 500-W is applied for varying periods of time, and the transparent solution changes color to dark shades of yellow or brown. Postcooling to room temperature the product is separated and purified. Particles obtained via this method have reported photoluminescent properties, which were exploited for various biomedical applications including photoacoustic imaging.<sup>67</sup> This is a facile, one-step procedure which is also environmentally friendly and cost-effective, rarely requiring further purification while producing homogeneous, spherical, and stable particles.

### 3.6 | Hydrothermal synthesis

This is a largely employed method quite popular due to the mild reaction conditions involved. Typically, the organic molecule precursors abundant in their N and O content (examples include glycine, TRIS, and EDTA among others) are heated at temperatures above 150°C in an autoclave for a few hours followed by cooling to room temperature, neutralization of the pH, extraction using organic solvents, and purification using dialysis. Special reactors made of stainless-steel outer and Teflon-coated inner lining resistant to conditions of high temperature and pressure are used. The particles thus produced have been reported to be homogeneous, spherical, highly hydrophilic,<sup>86</sup> with a high quantum yield<sup>87</sup> and stable up to a period of 2 months without any visible aggregation.<sup>88</sup> The diameters of particles thus prepared are lower than 10 nm.

### 3.7 | Solvothermal process

Solvothermal methods have been reportedly used to prepare CDs from various organic molecules as precursors. This method is popular for producing small particles, and CDs obtained via this method have been said to be crystalline with an average size of <5 nm. This process has been used to generate small-sized CDs with very high quantum yields and narrow fluorescence emission bands.<sup>26</sup> Various dopant-incorporated CDs from SiCl<sub>4</sub>,<sup>89</sup> NaNH<sub>2</sub>,<sup>90</sup> and BBr<sub>3</sub><sup>91</sup> have been fabricated by employing this process. In general, the starting materials are heated in an autoclave in conditions similar to the hydrothermal process (>200°C for a few hours).

### 3.8 | Pyrolytic method

This method involves heating organic precursors to high temperatures which are owed to their degradation. These reactions take place under an inert atmosphere, uses highly concentrated bases or acids, and have been reported by some researchers as an effective means of obtaining CDs.<sup>92,93</sup> The physicochemical changes that accompany thermal degradation lead to the formation of C rich residue. The synthesis of CDs with a size range of 2–3 nm, from a mixture of D-glucose and L-aspartic acid at a high temperature in the presence of NaOH was reported by Zheng and coworkers.<sup>94</sup> C sources as natural as watermelon and orange peels have been used to derive CDs using this method.<sup>95</sup> The optimization is obtained by controlling the temperature, acid concentration, and time of the reaction. Wang et al. reported the synthesis of CDs with a quantum yield of 53% using this technique.<sup>96</sup> Researchers also used varying passivation and capping agents to control the properties of the CDs thus obtained.

### 3.9 | Surface passivation and functionalization

The properties of CDs can be modified by functionalization of their surface. Surface passivation reduces the negative effect of surface contamination which would hamper their optical properties. Surface passivation is usually achieved by coating the surface of CDs using various linear or hyperbranched polymers like PEG and polyvinyl pyrrolidone, or small molecules like thionyl chloride and thiols, etc.<sup>97</sup> Since most CDs synthesized using several methods like the pyrolytic and chemical oxidation methods are not inherently fluorescent,<sup>98</sup> surface passivation is applied to increase their quantum yields and stabilize their fluorescence emissions. Surface passivation has been

reported to enhance the quantum yield of CDs by over 50%.<sup>99</sup>

Surface functionalization is used to add functional groups to the CDs to enhance certain properties like their biocompatibility or upconverted fluorescence. Various moieties like amines, thiols, and carboxyl are used for functionalization. They can be introduced using coordination chemistry, covalent conjugation, H-bonding, or  $\pi$ - $\pi$  interactions.<sup>69,100</sup> Due to the absence of bandgap absorptions in CDs the excited state energy trapping is attributed to the surface defects which influence the absorptions and emission intensities. Introduction of functional groups fill the defects on the surface, stabilize surface energy traps, and traps emission energy to the surface of the CDs due to the quantum confinement.<sup>101</sup> Functionalization can further control the size and aggregation properties of CDs.<sup>102</sup> Smaller the size, more stable the PL and greater the PL will be fluorescence quantum yield.<sup>101</sup>

In a research which was the first of its kind, Pan and coworkers reported the synthesis of CDs functionalized with various amino acids using 1-ethyl-3-(3-dimethylaminopropyl)carbodiimide/N-hydroxysuccinimide (EDC/NHS) coupling which flipped the chirality of cyclic  $\alpha$ -amino acid (Figure 5). The functionalized CDs were also found to selectively interact with cellular membranes, and these materials were proposed for use as investigative agents for various cellular trafficking pathways.<sup>103</sup> The group also reported another study where sparteine was used as a surface passivation agent for use of decorated CDs as an enantioselective separation platform for representative racemic mixtures.<sup>104</sup> Further, the group also reported the synthesis of chiral carbon nanoparticles capable of targeting the DNA in cancer cells. They achieved enantiospecific DNA recognition by controlling the attachment of Tröger's base used as a groove binder on breast cancer MCF7 cells.<sup>105</sup>

### 3.10 | Synthesis of carbonized polymer dots

Generally, CQDs and GQDs are achieved by top-down methods. Only postdecoration with suitable polymer or organic molecules can transform them into CPDs having an unambiguous carbon core and a polymer shell.<sup>106</sup> Bottom-up approaches, on the other hand, are the most common routes to produce CPDs.<sup>13</sup> They primarily originate from various polymeric precursor or small molecules which undergo dehydration followed by carbonization to generate CPDs. The bottom-up methods for the preparation of CPDs include hydrothermal, solvothermal, and microwave-assisted hydrothermal/solvothermal, etc.<sup>107–112</sup> Importantly, CPDs not only exhibit the traditional optical

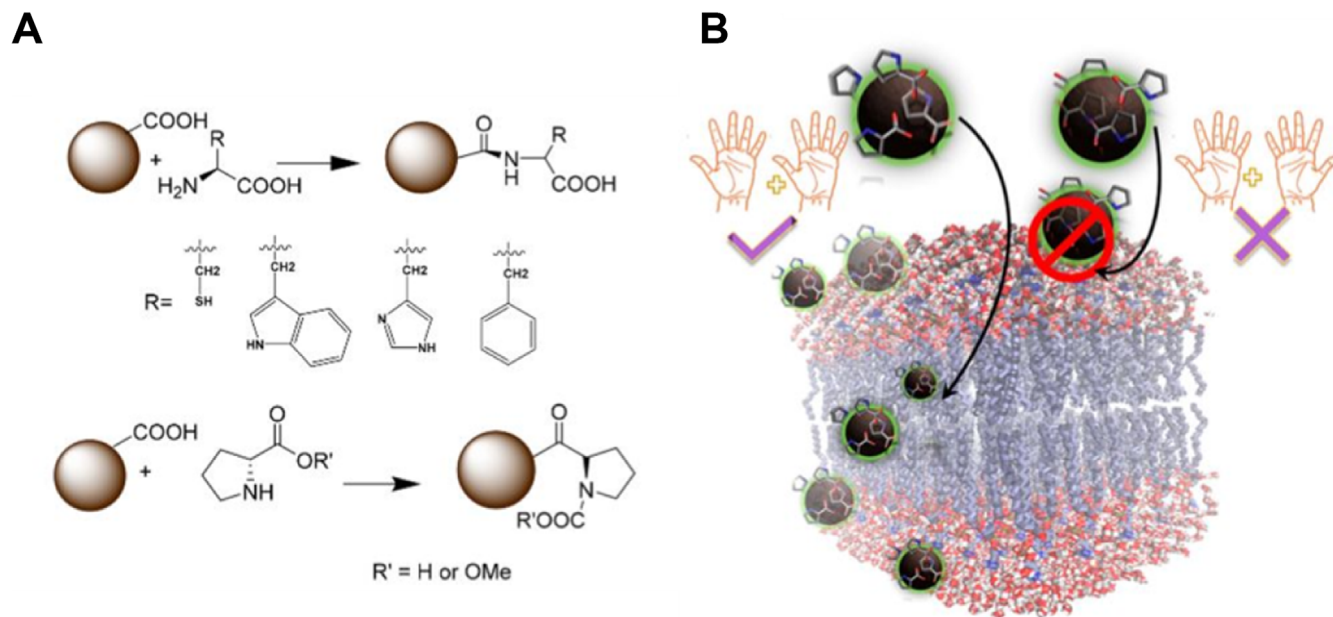


**FIGURE 5** (A) Synthetic scheme for the synthesis of amino acid-functionalized CDs and (B) graphical representation of the covalent surface conjugation of cyclic  $\alpha$ -amino acid causing asymmetric chiral inversion. (Reprinted with permission from Ref. 103)

properties of CDs but also possess the polymeric characteristics. The polymeric properties generally evolve from three aspects in CPDs. First are the abundant surface functional groups and short polymer chains which remained due to the incomplete carbonization. Second is the polydispersity in structure and property which are imposed either by improper reaction conditions or complex polymerization process. Lastly, dehydration and carbonization develop highly cross-linked structures in CPDs in contrast to other CD variants.<sup>113</sup>

Table 1 summarizes the various methods and precursors used to synthesize CDs and their sizes thus obtained.

## 4 | APPLICATIONS OF CDs

The past decade has witnessed a surge in research involving carbon dots not only due to the facile synthetic methods available but mainly due to their versatile applications ranging from sensing to drug delivery. This section will include an overview of the various domains in which CDs have been used.

### 4.1 | Applications of CDs towards disease diagnosis: Bio-imaging platform

Owing to their unique photoluminescent properties, CDs have been marketed as ideal candidates for various imaging applications. The fluorescent properties of CDs

are controlled by the synthetic route employed, their size, shape, and surface functionalization as well as the excitation wavelength.<sup>127</sup> To tune these properties to enhance their applications as imaging agents, their fluorescence in the NIR (near-infrared region) has been exploited to nullify the background fluorescence captured from red blood cells.<sup>128</sup> By varying the excitation wavelength, the fluorescence emission of CDs can be widely varied to produce blue, red, and green fluorescence and thereby used as a multicolor probe.<sup>14,129</sup> Although a number of dyes and fluorophores are available as imaging agents, their biocompatibility, clearance, and low aqueous solubility make them less attractive as compared to CDs which have a wide range of tunable properties and have largely reported to have no cytotoxic effect. The ideal agent for imaging applications is desired to exhibit low toxicity, high accumulation, and biocompatibility.

#### 4.1.1 | Optical bioimaging

There has been considerable focus on harnessing the unique optical properties of CDs to use them for applications in optical imaging.<sup>130</sup> Conventional organic dyes, quantum dots with heavy metals, and other agents lag behind due to their potential toxicity as well as low quantum yield and photobleaching.<sup>128</sup> CDs have tunable fluorescence properties which can be optimized by varying their method of preparation as surface passivation.<sup>131</sup> Fluorescent water-soluble carbon nanoparticles with an

**TABLE 1** List of various synthetic routes used for the generation of CDs

Precursor	Method	Type of CD	Size (nm)	References
Graphite powder	Laser ablation	Carbon nanodot	1.5–1.8	114
Toluene	Laser ablation	Carbon dot	2–20	115
Ethanol	Electrochemical process	Carbon nanodot	2.1–4.3	73
Sodium citrate	Electrochemical process	Carbon dot	1.0–3.5	74
Graphite powder	Ball milling	Graphene quantum dot	210	116
Cellulose	Ball milling	Carbon quantum dot	2–8	117
Ascorbic acid	Ultrasonication	Carbon quantum dot	3–4	81
Citric acid	Ultrasonication	Graphene quantum dot	1.8–3.8	41
Glucose	Ultrasonication	Carbon dot	10	118
Glycerol	Microwave irradiation	Carbon dot	5	119
Triammonium citrate	Microwave irradiation	Carbon nanodot	6.5	120
Arginine	Microwave irradiation	Carbon dot	1–7	121
Xylose	Microwave irradiation	Carbon dot	1.8	83
Watermelon peel	Hydrothermal	Carbon dot	2	122
Chitosan	Hydrothermal	Carbon quantum dot	2	123
Spices	Hydrothermal	Carbon dot	3.4–4.3	124
Hydroquinone	Solvothermal	Carbon quantum dot	16	91
Melamine	Solvothermal	Carbon dot	4–10	125
potassium peroxydisulfate, <i>N,N'</i> -methylenediacrylamide, AIBN	Hydrothermal	Carbonized polymer dots	4.56	107
Branched polyethylenimine	Cross-link immobilization	Carbonized polymer dots	63	110
Poly(vinyl alcohol)	Hydrothermal	Carbonized polymer dots	2–7	126
Citric acid and polyamine	Microwave	Carbonized polymer dots	5	111
Dopamine ando-phenylenediamine	Hydrothermal	Carbonized polymer dots	7.8	112

average size of 5 nm exhibiting blue and yellow fluorescence were found to internalize in HepG2 cells<sup>54</sup> (a human liver cancer cell line) while photoluminescent CDs both in solid-state and solution, uptaken by Caco-2 cells (human epithelial colorectal adenocarcinoma cell line) was first reported in 2006.<sup>71</sup> Mehta et al., used potatoes as a starting source for the synthesis of CDs with multicolor emission and found their internalization in HeLa cells.<sup>132</sup>

In a recently published study, Pan and coworkers have investigated the energy flow and excited-state dynamics between and within CDs (Figure 6). The authors observed the electron–photon dynamics via optical excitation. The temporal resolution of their studies was at a scale of 0.1–500 ps and a spatial area of 1 nm<sup>2</sup>. The excited state dynamics was found to vary largely, with some relaxing much faster than the others, where the energy is localized and remains in the surface states for enhanced periods.<sup>133</sup> The combined effect of these two states gives rise to the unique fluorescence yields that make CDs so attractive for imaging and theranostic uses.

Apart from in vitro imaging, the use of CDs for in vivo imaging has also been investigated by varying different parameters including the routes of administration,

excitation wavelengths, and source of precursors.<sup>67,134</sup> Pan and coworkers demonstrated the efficiency of CDs using intradermal administration of CDs passivated with hyperbranched for mapping sentinel lymph nodes<sup>67</sup> within 1 min postinjection with high enhancement of contrast and no off target toxicity. Hyperbranched polymers have been used widely for various biomedical applications including drug delivery agents due to their unique condensed 3D structures mimicking those of proteins, intrinsic molecular confinement capabilities, and their inertness to various the biological components.<sup>135</sup> Various modes of injections of CDs (subcutaneous, intradermal, intravenous) have shown them to retain their strong fluorescent properties and prove their potential as a biocompatible imaging agent<sup>136</sup> (Figure 7).

#### 4.1.2 | Raman and hyperspectral imaging

Raman scattering involves the gain of vibrational energy when photons from the source shift to a lower level. This is an inelastic type of scattering where the emission wavelength is shifted due to light excitation and not PL.<sup>137</sup> When



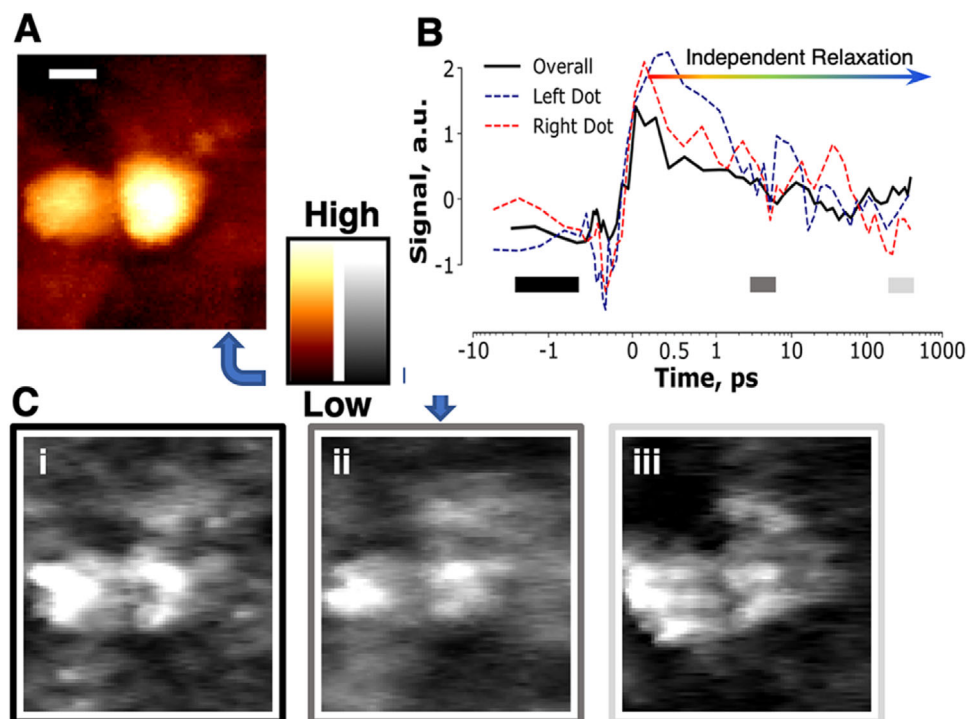


**FIGURE 6** Observation of independent relaxation and energy transfer by surface-mediated heat flow between blue carbon dots. (A) Topographic image of two CDs with independent relaxation and (B) pump-probe traces for both dots (solid black line) and each individual dot (dashed lines). Independent relaxation of each dot is indicated by the rainbow arrow. The gray bars indicate the time range for the images in (C). (C, i-iii) trSMA-STM images; (Cii) and (Ciii) show evidence of general surface heating from 5 to 200 ps (reprinted with permission from Ref. 133)

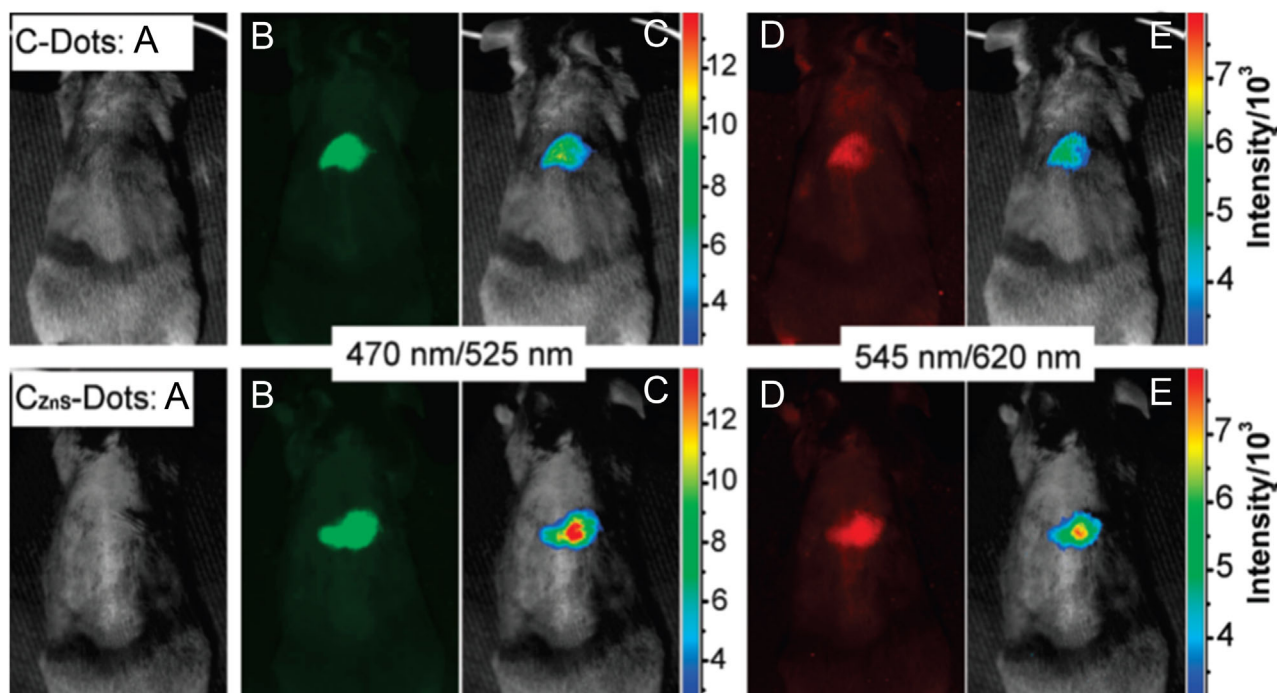


**FIGURE 7** CDs retaining their fluorescent characteristics postsubcutaneous injection of (top) CDs and (bottom) CZnS-dots: (A) bright field, (B, D) as-detected fluorescence (excitation/emission wavelengths indicated), and (C, E) color-coded images. (Reprinted with permission from Ref. 136)

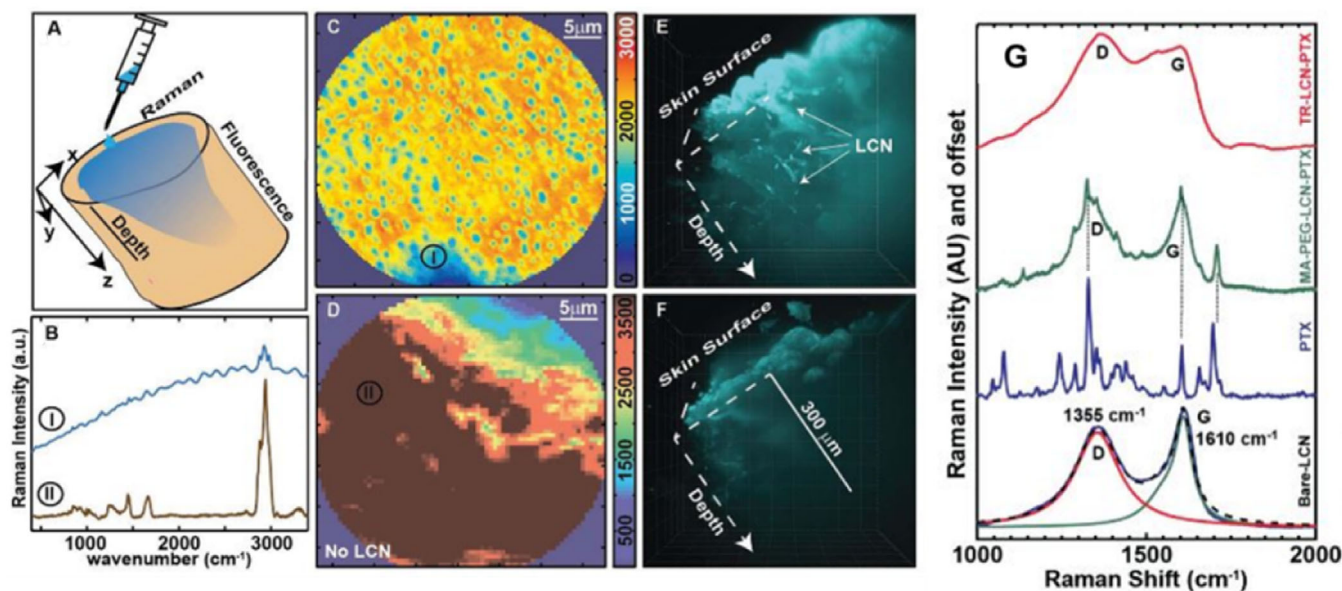


**FIGURE 8** (A) Schematic representation showing imaging strategies for the pigskin surface and depth penetration inside pigskin; (B) shows the average Raman spectra of CDs on the skin(I) and untreated skin (II); (C) and (D) images formed by integrating the area under the C-H peak at approximately  $2900\text{ cm}^{-1}$  after baseline correction for the treated and untreated skin, respectively; (E) and (F) 3D light-sheet fluorescence images of CD treated and untreated pigskin biopsies; (G) Raman spectra of free CDs, free drug, and drug-loaded CDs. Characteristic D and G bands are observed which make them Raman active and used for skin depth penetration monitoring. (Reprinted with permission from Ref. 141)

the laser energy reaches the desired value, required for the electron to transit from the valence band to the conduction band, the generated signal is referred to “resonance Raman scattering.”<sup>138</sup> In comparison to fluorescence-based imaging methods, surface-enhanced Raman scattering (SERS) has narrower spectral bands and is more sensitive in its detection and quantification.<sup>139</sup>

The SERS effect is a surface phenomenon linked to the excitation of the surface plasmon resonance or SPR band. This increases the electric field which is harnessed for various imaging techniques. The modification of surfaces can enhance this phenomenon and lead to increased sensitivity.<sup>140</sup> Due to the presence of D and G bands, CDs have been used for Raman imaging in live cells. The presence of these bands allows for scattering which in turn provides a multicolored imaging platform.<sup>128</sup> Raman spectroscopy provides both lateral and confocal high-resolution images and can be used in aqueous solutions. The Pan group harnessed this property to track CDs loaded with chemotherapeutics in cells.<sup>141</sup> They reported the synthesis of CDs with modified surface activity by using surface agents with emission spectra in the visible and NIR region. The Raman active nature of the CDs allowed their monitoring on the surface of the skin using 3D fluorescence imaging (Figure 8).

The fluorescence emission of CDs is sensitive to changes in the environment and can be assessed by measuring

the change in the intensity, wavelength, or bandwidth. and Carbon nanotube fluorescence responds to its environment via changes in intensity, wavelength, or spectral bandwidth.<sup>142</sup> The emission bands corresponding to each unique species and can be used to image several spectrally separated emitters.<sup>143</sup> The Pan group reported the synthesis of drug-loaded CDs lesser than 30 nm in size using prodrug passivated CDs and employed hyperspectral imaging to map and quantify the drug-loaded nanocarriers<sup>144</sup> (Figure 9). Their pioneering work provided a platform for the spatiotemporal characterization and simultaneous detection of the drug and the vehicle.<sup>144</sup>

#### 4.1.3 | Magnetic resonance imaging

Magnetic resonance imaging (MRI) is a popular imaging tool in clinical settings owing to its noninvasive nature and penetration depth. The main function of a contrast agent is the reduction of the relaxation times ( $T_1$  and  $T_2$ ) of protons thereby enhancing the image contrast.<sup>145</sup> The major limitations of currently employed contrast agents include high toxicity, low sensitivity, reduced half-life.<sup>146</sup> When selecting a contrast agent for MRI, its size is of prime importance as large size particles has been reported to accumulate in the spleen and liver. The relaxation times

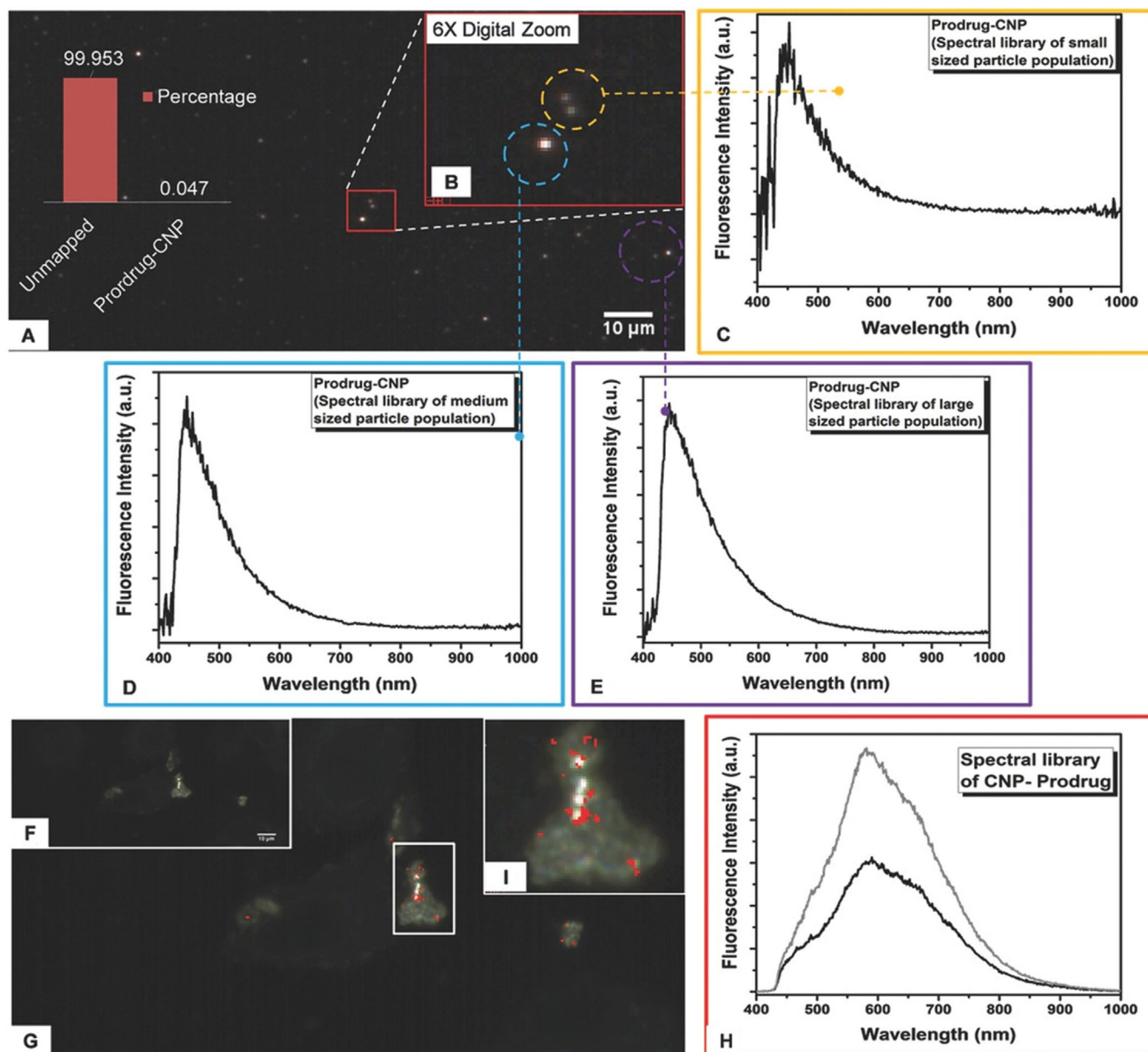


**FIGURE 9** Hyperspectral imaging showing prodrug-CDs inside MCF-7 cells after 4 h of incubation. Imaging was performed on prodrug-CNP particles in (A–E) solution phase and (F–I) inside the cells. (A) Prodrug-CDs clusters in aqueous solution imaged under a hyperspectral microscope and (B) image at 6× optical zoom. Fluorescence spectra generated from particle clusters of (C) small, (D) medium, and (E) big size. Intracellularly located prodrug-CNPs imaged at photoluminescent 1× and (G) 6× optical zoom and respective spectral library (H). (I) Distribution of prodrug-CNP visualized in the cellular background with 0.047% of covering area. (Reprinted with permission from Ref. 144)

and optical properties to enhance contrast and cytotoxicity are also key parameters that make CDs attractive for their use as imaging probes for MRI imaging. High fluorescence quantum yields and the possibility of attaching a targeting ligand and doping them with elements to control the contrast as well as the longitudinal relaxivity are reasons why CDs have been proposed as prospective agents for such techniques. Several doped CDs have been reported as efficient probes for imaging applications. Gd-doped

C-dots with high fluorescence quantum yield and a longer relaxation time have been reported by various research groups.<sup>147,148</sup> The brightness is enhanced by increasing the Gd concentration, and these nanomaterials have thus been proposed for use as positive MRI contrast agents. As a more biocompatible and cost-effective alternative to Gd, Mn has been used as a dopant and these CDs have been reported to exhibit properties similar to their Gd-doped counterparts.<sup>149</sup>



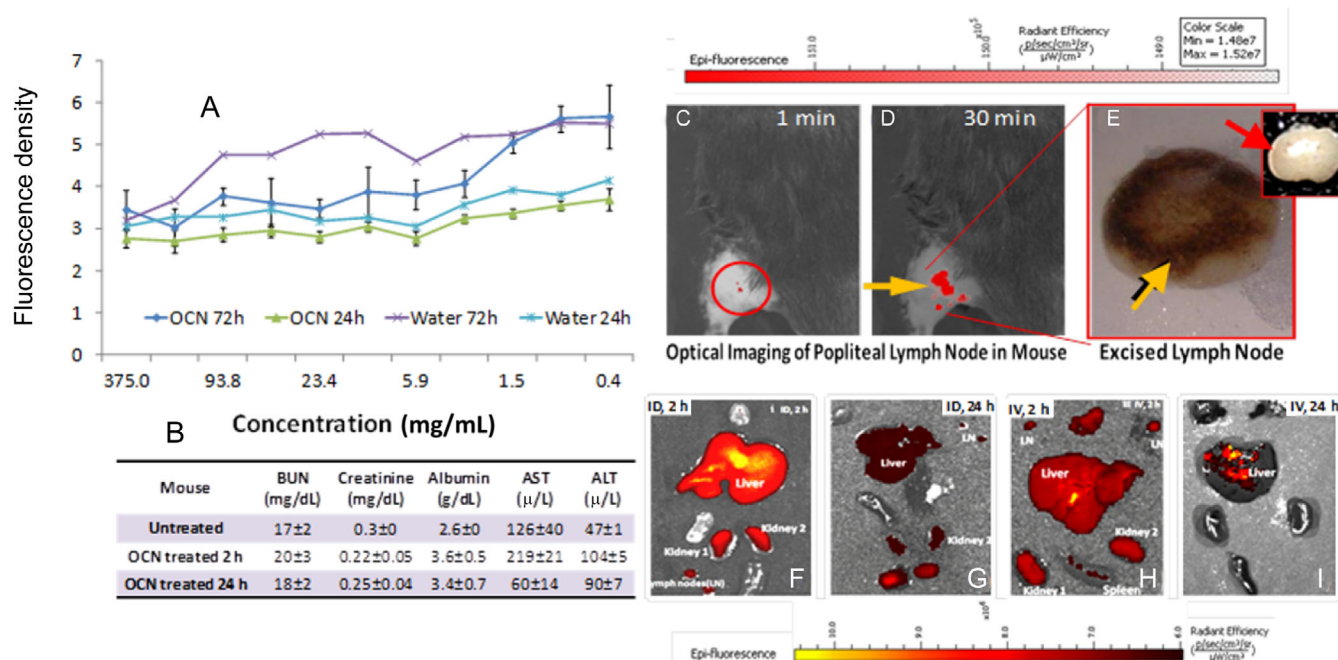


**FIGURE 10** (A) Cell viability of optically active carbon nanoparticle (OCN) in 2F2B endothelial cells; (B) clinical pathology and serum chemistry results for OCN among untreated and treated mice for a different duration. Noninvasive in vivo fluorescence imaging in mouse: fast accumulation of OCN in popliteal lymph node postinjection (C) 1 min and (D) 30 min; (E) excised lymph node showing the accumulation of dark deposit of carbon particles (yellow arrow). A control excised lymph node from untreated mice showing no visible accumulation of OCN could be seen from the inset. Qualitative tissue distribution of OCN: after 2 h (F, G) and 24 h (H, I) was recorded by tissue accumulation of intradermally and intravenously injected OCN. (Reprinted with permission from Ref.97)

#### 4.1.4 | Photoacoustic imaging

Photoacoustic (PA) imaging is an imaging technique that makes use of laser-generated ultrasound signals. It combines the high-contrast and spectroscopic-based specificity of optical imaging with the high spatial resolution of ultrasound imaging. The contrast of the images thus generated depends on the optical absorption of the biological tissues. It is a very sensitive modality that has been used for the detection of various small molecules like water and biological agents like lipids and hemoglobin.<sup>150</sup> Since CDs exhibit strong absorption in the NIR region and their size is optimal for lymphatic transport, they have been used as exogenous contrast agents for PA imaging.<sup>101,151</sup> Using CDs derived from honey as a precursor, Pan and coworkers used these nanomaterials to effectively image SLN. Once injected these small CDs were transported swiftly to the axillary thereby enhancing the clarity of the node.<sup>67</sup> They also demonstrated the capability of optically active carbon nanoparticles for noninvasive in vivo fluorescence imaging in mouse and especially their biodistribution in lymph node (Figure 10).

Table 2 highlights the different types of imaging modalities achieved using CDs along with their source and area of application.

#### 4.2 | Applications of CDs towards disease diagnosis: Biosensing platform

The photoluminescent and electronic and size-dependent properties of CDs make them attractive agents for various sensing applications including chemical, biological, and electrochemical sensing.<sup>57,108,160</sup> Their unique “turn on–turn off” feature is primarily due to FRET (fluorescence resonance energy transfer), charge transfer, and inner filter effect<sup>161</sup> and allows for their use as sensors for biological molecules and metal ions.<sup>162</sup> Metal nanoparticles have been studied in depth for their unique size-based colorimetric properties based on the SPR effect.<sup>163</sup> Metallic and bimetallic nanoparticles stabilized via a host of organic and inorganic ligands have been used for sensing applications, but certain drawbacks including aggregation and inherent toxicity.<sup>164</sup> CDs, on the other hand, present attractive PL and biocompatible features including intense fluorescence emission and fluorescence quenching when bound to target analytes, presence of targeting sites, variable emission spectra, and minimal cytotoxicity and are thus being considered as alternative options to pre-existing sensing probes.<sup>49,165</sup>

Sensing of different anions, proteins, biomolecules based on fluorescence is a field of study gaining



TABLE 2 CDs used in various imaging applications

Source	Application	Used in	Reference
Citric acid	Optical Imaging	HepG2, HeLa	19
Carbon soot	Optical Imaging	HepG2	54
Glycine	Optical Imaging	MCF-7	86
Folic acid	Optical Imaging	U87 glioma cells	152
Graphite	Two-photon imaging	HeLa, HEK 293T	153
Glucose	Two-photon imaging	DU145	154
Polydimethylsiloxane	SERS imaging	Bacterial strains	155
Polythiophene phenylpropionic acid	Photoacoustic imaging	HeLa, nude mice	156
Hypocrella bambusae	Photoacoustic imaging	HeLa, nude mice	157
Citric acid, urea	Photoacoustic imaging	4T1, HepG2, HeLa, nude mice	158
Graphite	NIR imaging	Nude mice	159
Citrate acid, ethanediamine GdCl <sub>3</sub>	MRI imaging	U87, Live mice	148

considerable attention. This method generates an output based on the differences in optical patterns from a sensor. CDs have been used to develop such smart sensors to detect and differentiate various biomolecules with high sensitivity and extreme accuracy.<sup>166</sup> Machine learning algorithms have been clubbed with this to generate a method capable of performing more accurately and effectively than conventional statistical pattern recognition techniques.<sup>167</sup>

Based on the multicolor fluorescence of CDs owing its origin in all probability to different surface defects and energy traps. Ratiometric sensing using the surface modification of certain substances to induce FRET coupling is also used for the detection of small molecules.<sup>145</sup> CDs materials have been used in the detection of various important biomolecules which are important for the early diagnosis of several diseases.

Glutathione (GSH), is one of the most prevalent cellular biothiols and maintenance of its optimal level in the body is responsible for defense against toxins and free radicals.<sup>168</sup> Abnormal levels of GSH have been reported to be associated with various types of cancers.<sup>169</sup> A major complication in the detection of GSH is its structural similarity with the amino acid cysteine (Cys) and homocysteine (H-cys).<sup>170</sup> Gupta and coworkers reported the facile synthesis of multicolor fluorescent CDs doped with sulfur for naked-eye colorimetric detection for GSH and arsenic with a high level of sensitivity<sup>2</sup> (Figure 11). The synthesized CDs were also able to detect GSH in the presence of like Cys and H-cys with a detection limit (DL) of 43 nM, even in blood plasma.

Tripathi et al. used chiral CDs with a size of 20 nm for sensing DNA using the chiral property of the CDs which was induced by using Tröger's base (TB). The CDs enriched the nucleus in MCF-7 cells while the negatively chiral

CDs were found to inhibit cell viability on the same cell line. These particles were reported to act as tweezers on genomic DNA and caused apoptosis in a cascade effect.<sup>105</sup>

### 4.3 | Applications of CDs towards the delivery of therapeutics

CDs have become a popular choice as drug delivery agents<sup>128,171</sup> along with metal nanoparticles,<sup>172</sup> polymersomes,<sup>173</sup> and other molecules.<sup>174,175</sup> Their salient features which include hydrophilicity, biocompatibility, surface functionalization, traceability due to inherent fluorescent properties, and small size make them attractive candidates for the delivery of therapeutic drugs and their use as theranostic agents.<sup>44,62,93,136,140,141,145,174,176,177</sup> Table 3 summarizes the various uses of CDs in the biomedical field along with their precursor sources.

Harnessing the properties of CDs to achieve controlled and targeted release has shown promise in the treatment of various diseases including cancer. Furthermore, their intrinsic fluorescence properties are exploited as alternatives to organic dyes thereby allowing for their tracking in the system. Although polymersomes, liposomes, and other nanoparticles have been investigated for their applications as drug delivery agents, their multistep synthesis, use of organic solvents, low drug loading, inherent cytotoxicity, and batch-to-batch variations. CDs have various attractive features as compared to their other nanosized counterparts which have made them stand out in the field of drug delivery and therapeutic carriers.

The Pan group has done pioneering work in the use of CDs for simultaneous imaging and delivery using CDs. In 2015, the group reported the use of CDs whose surface was functionalized to generate a thermoresponsive model

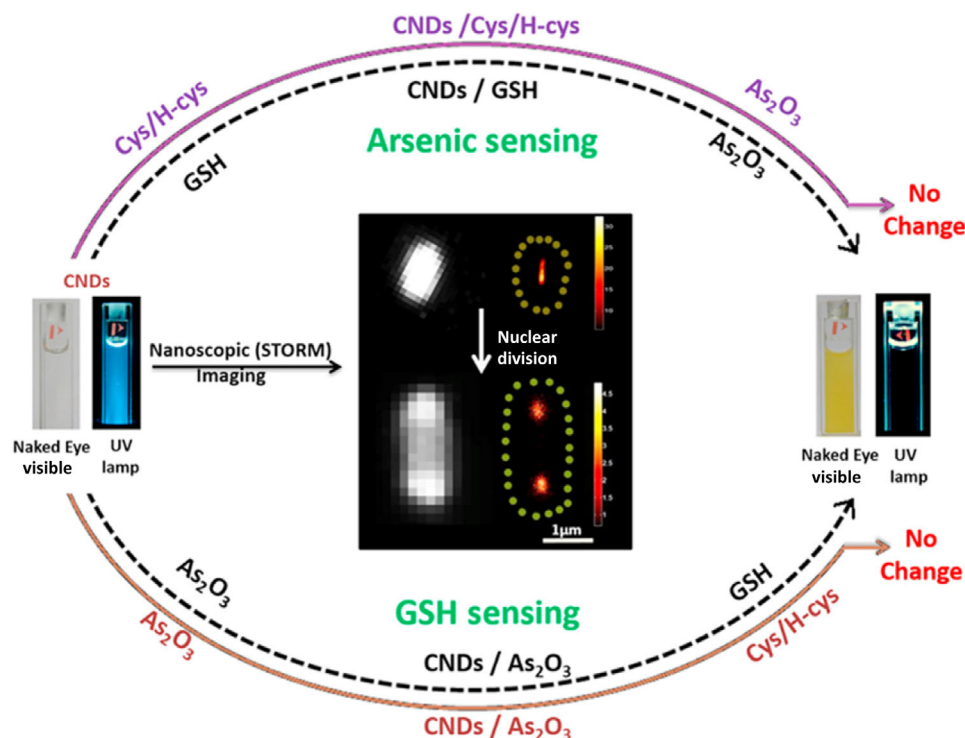


**FIGURE 11** Schematic representation showing the use of CDs as a single platform for the detection of glutathione and arsenic. Reprinted with permission from Ref. 2

**TABLE 3** CDs used in biomedical applications

Source	Application	Cell line	Reference
Citric acid, ethylenediamine	Drug delivery	L929, MCF-7, CCK-8	180
Diaminohexane, Hyaluronic acid	Photodynamic Therapy	B16F10	181
Glycerol	Gene transfection	HeLa, PC-3	182
Glucose	Drug delivery	DUI45, C57BL/6	154
Ferrocene	Drug delivery	B16F10	183
Citric acid and tryptophan	Gene transfection	MGC-803	184
Citric acid	Drug delivery	A2780	185
Carbon soot	Photodynamic Therapy	MGC803	186
Citric acid, polyene polyamine	Drug delivery	HepG2	19
EDTA	Drug delivery	HeLa	187
ATP, hyaluronic acid	Drug delivery	HeLa	188
Sucrose	Photothermal therapy	MCF-7	189
Agave nectar	Gene transfection	MDA-MB-231, MCF-7	190
Carbon nanopowder	Drug delivery	CHLA-266, SJGBM2	191

(TE-LCN) or passivated using a multiarm PEG moiety. The release profile of the PEGylated system was more efficient in terms of controlled release and loading content and was thus chosen for therapeutic applications. The fluorescent properties of the CDs were also used for ex vivo imaging, and the results concluded the promising applications of the synthesized materials for in vivo imaging applications.<sup>141</sup>

The following year the group presented a one-step multifunctional platform for cellular internalization and uptakes of the CDs.<sup>178,179</sup> The authors used carotene to harness its visible absorbance features to be able to trace the nanosystems at the same time exploit the intrinsic antioxidant and antimetastatic properties of  $\beta$ -carotene and finally layering CDs with a phospholipid to achieve

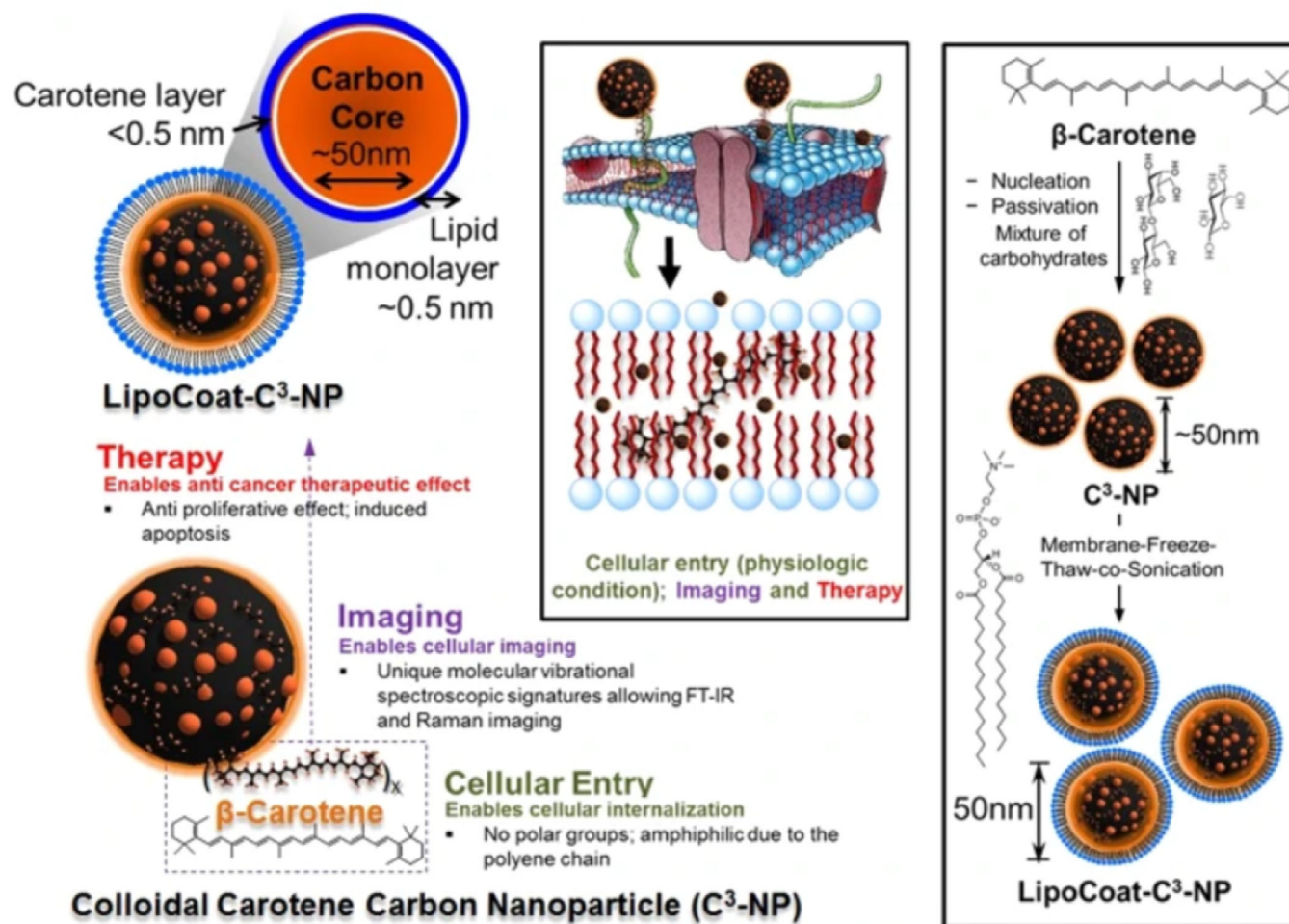


FIGURE 12 Schematic representation of the use of CDs harnessed with carotene for a single platform to achieve synchronous imaging, cellular uptake, and therapy. (Reprinted with permission from Ref. 178)

facile cellular uptake (Figure 12). When tested on two different cell lines, human skin melanoma cells (C32) and triple-negative breast cancer MDA-MB 231 cells, the CDs presented a significant reduction in the IC<sub>50</sub> values as compared to free  $\beta$ -carotene. A temperature-dependent cellular uptake was also observed with minimal uptake at lower temperatures which increased significantly at 37°C. When used as imaging probes on the skin, the authors found an enhanced contrast clearly distinguishable from the autofluorescence.

In another study, citric acid and ethylenediamine were used to fabricate CDs using the hydrothermal approach and conjugated with doxorubicin to validate their therapeutic efficacy. The cellular uptake and viability were measured on L929 and MCF-7 cells. This study revealed high drug loading of the CDs and enhanced cellular uptake and mortality as compared to the free drug (Figure 13).<sup>180</sup>

## 5 | CURRENT CHALLENGES WITH THE USE OF CARBON DOTS

Although CDs have presented themselves as ideal candidates in a multitude of domains, there are still concerns regarding their usage in certain applications and their efficiency as replacements to preexisting systems. As mentioned earlier, the photoluminescent properties of CDs are key features used to develop CD-based sensors and ECL sensors and permit their use in PV cells. However, the detection of phosphorescence and debatable up-converted PL are some challenges that need to be overcome. These effects may be due to their internal structure which lies between amorphous and semicrystalline and their polydispersity in size.<sup>176</sup> The use of CDs in electrocatalysis for oxygen reduction reaction has not been explored to a full-depth due to limited knowledge of their electrocatalytic activity.

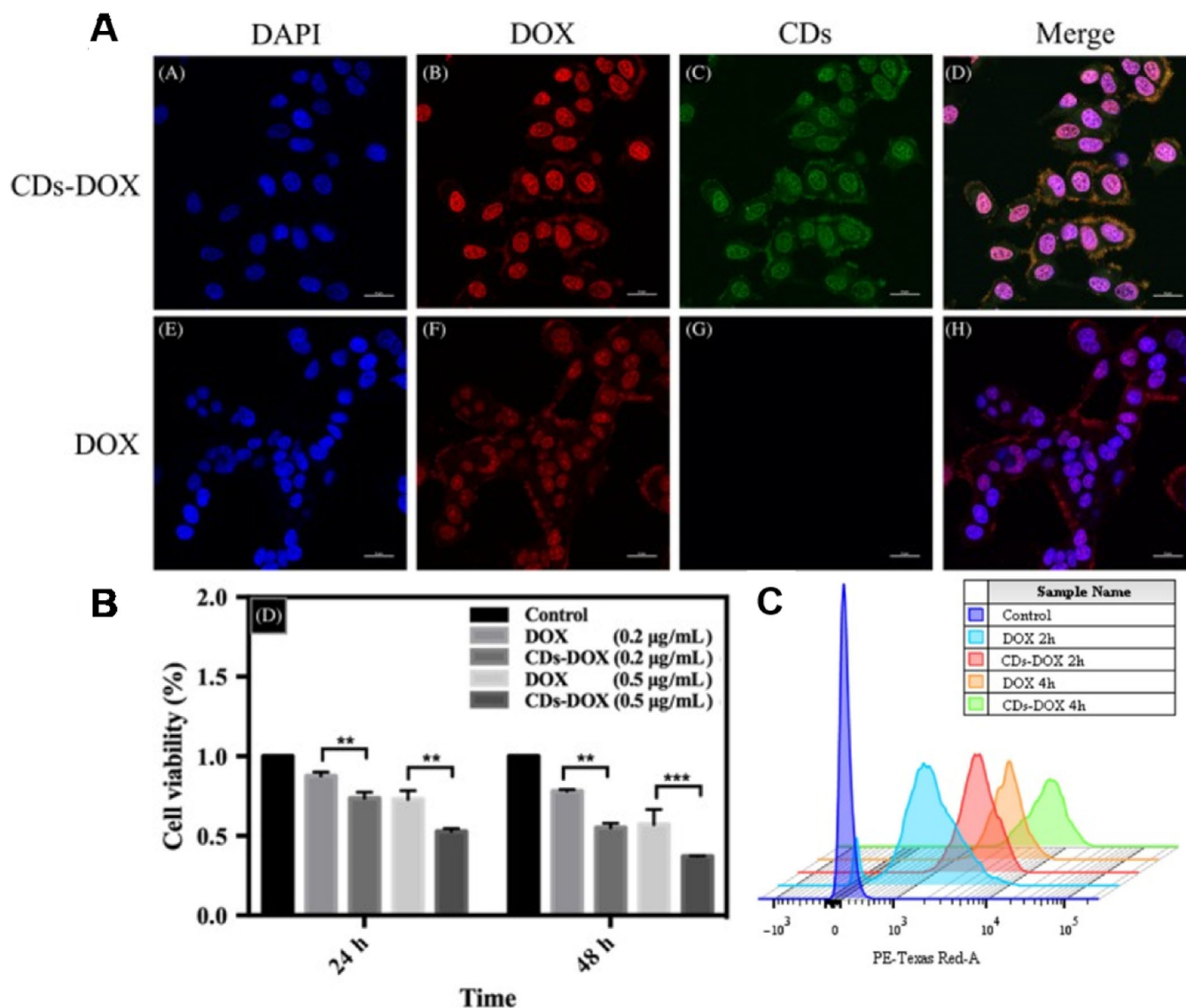


**FIGURE 13** (A) Confocal microscopy images of MCF-7 cells incubated with CDs-DOX and free DOX. The cell nuclei (stained with DAPI), DOX, and carbon dots exhibited blue, red, and green fluorescence, respectively. The scale bars are 25 µm in all the images. (B) Cell viability of free DOX and CDs-DOX on MCF-7 cells at 24 and 48 h showing enhanced killing efficiency of the CDs, and (C) 3D flow cytometry histograms of cells after 2 and 4 h postincubation showing increased uptake of CDs-DOX. (Reprinted with permission from Ref. 179)

Another key factor that needs to be addressed is the large-scale synthesis of CDs. Till now only gram-scale synthesis has been reported which needs to be scaled up while maintaining reproducibility of the process and maintaining the intactness of their physicochemical properties.<sup>145</sup> Mechanistic insights into the formation of CDs are still lacking which is a key feature in controlling their surface and size-dependent properties.

The size distribution of CDs plays a vital role in governing key features like toxicity and fluorescence emission. Uniformity in this regard is a challenge still unmet. Although PL is a much studied and exploited feature of CDs their wide range emission spectrum needs to be fine-tuned for better control of their optical properties. Most

CDs are either blue or green although NIR emission has also been reported in certain cases. The development of IR and NIR emissive CDs is desirable for deep tissue imaging. Furthermore, the quantum yield of CDs in the absence of external surface enhancements is low.<sup>192</sup> A major area of interest for CDs is their applications in vivo. However, certain reports have shown their rapid hepatic and renal clearance which may primarily due to their small size. Design of CDs that degrade in situ or better control of the size of CDs may help improve their plasma half-life and circulation times.

Overall, the primary factors that control the selective theranostic applications of graphene and CQDs, CDs with dopants, and amorphous CDs are (i) toxicity;



(ii) biodistribution and circulation time; and (iii) photobleaching.<sup>193</sup> First, the cellular viability of CD variants depends on the cell type under investigation and its dosage amount.<sup>194</sup> It is thus known that the elementary cause of toxicity is the interaction of cells with CDs and shrinkage of cells and holes on their surface.<sup>195</sup> Hence, surface charge on CDs plays a crucial role in their toxicity evaluation. Accordingly, Yuan et al. investigated the role of different surface functional groups (COOH, NH<sub>2</sub>, and CO-N(CH<sub>3</sub>)<sub>2</sub>) towards the cellular viability of GQDs on human A549 lung carcinoma cells. On the other hand, polymer coatings had been demonstrated to modify the toxicity of CDs.<sup>196,197</sup> Further, a number of parameters like size, solubility, morphology, surface functional groups, pH, and environmental factors strongly trigger the level of reactive oxygen species (ROS) in CD variants which is one of the prime causes of their cellular toxicity. Smaller sized NPs can easily enter cells, but they are relatively more toxic. Morphology also plays an important role, and it was demonstrated that a larger contact area increases biocompatibility.<sup>198</sup> Separately, while evaluating the role of surface coating on ROS generation, Hoskins et al. showed that neutral PEG) coating had a lower ROS level than the positively charged polyethylenimine.<sup>199</sup> Second, the biodistribution of CDs is a crucial parameter to determine their circulation under in vivo conditions and the size of nanoparticles is an important feature that contributes towards this. It was demonstrated that smaller nanoparticles were more stable with longer circulation in the body.<sup>200</sup> Most of the nanoparticles are cleared via the renal pathway with minimal liver uptake, while the mononuclear phagocyte system and reticuloendothelial system are the two major mechanisms for nanoparticles' clearance.<sup>201</sup> Surface charge also plays a crucial role in the biodistribution of CDs. Negatively and positively charged CDs generally accumulate in the liver due to their tendency to adsorb protein and form a corona. Neutral and zwitterionic CDs, on the other hand, mostly accumulate in the kidney and are cleared by renal filtration as they do not form any significant protein corona.<sup>201,202</sup> Although the in vivo stability of CDs is not much impressive, their photostability is quite intriguing. It was found that PL of quaternized CDs was stable even up to 2 weeks with minimal photobleaching.<sup>203</sup> Overall, the duration of light exposure and concentration of CDs, and the presence of oxygen are the primary parameters that influence the photobleaching of CDs. Hence, intelligent manipulation and selective control of the various physiochemical properties, such as size, chemical groups, dopants, edge configurations, defects, and shape, are necessary to manifest efficacious theranostic applications

of graphene and CQDs, CDs with dopants, and amorphous CDs.

## 6 | FUTURE PERSPECTIVE

The emergence of CDs as a new class of nanomaterials is a relatively nascent field with ample opportunities of improving their features and maximize their utilization through detailed investigation of their properties. An important factor needing consideration would be their commercial-scale synthesis with a uniform size distribution, without compromising any salient feature. Modification of surface chemistry, and functionalization will open new horizons for further applications as imaging agents and sensors. Decorating their surface with magnetic NPs would enhance their use as MRI agents and targeted drug delivery and therapy.

The use of CDs in the storage and electron transport under visible light is also a less explored area of research so far. Improvements in the photocatalytic activity of CDs may also create a breakthrough in energy consumption and conservation which continues to be a global crisis. Their employment in the field of optoelectronics may also provide the industry with an economic solution. Exploiting the PL and properties further for rendering them useful in LEDs and improving the luminescence of lighting agents with lower energy consumption and carbon footprint is also an area that could be explored.

The immense potential of CD as sensors for various molecules and ions has been reported in-depth, but their role in the detection and sensing of various toxic metals like Cd<sup>2+</sup> and As<sup>3+</sup> has still not been explored to its full potential. This is an important aspect for environmental and health safety applications.

CDs are employed in drug and gene delivery for their biocompatible and unique PL features. However, a combined delivery platform for the codelivery can be designed to further enhance this field as already achieved for imaging and drug delivery.<sup>178</sup> A better understanding of their exact mechanism of in vivo biodistribution, cellular uptake, and long-range toxicity profile still require in-depth analysis<sup>204</sup> to improve their pharmacokinetics/pharmacodynamics (PK/PD) profile and enhance penetration into low vasculature and deep-seated tumors.

Addressing the aforementioned challenges through detailed insights into the working of CDs and modification of their features would further enhance their contribution in the biomedical and energy fields which would benefit mankind immensely by providing greener and cost-effective solutions to several major areas of concern. These

small particles have enormous potential and the future looks glowing brightly on the horizon of CDs.

## CONFLICT OF INTEREST

D.P. is the founder/cofounder of three University-based start-ups. None of these entities, however, supported this work. All the authors thus declare no competing interests.

## ACKNOWLEDGMENTS

The authors acknowledge the receipt of funding from the University of Maryland Baltimore and University of Maryland Baltimore County.

## ORCID

Dipanjana Pan  <https://orcid.org/0000-0003-0175-4704>

## REFERENCES

1. R. Das, R. Bandyopadhyay, P. Pramanik, *Mater. Today Chem.* **2018**, *8*, 96.
2. A. Gupta, N. C. Verma, S. Khan, C. K. Nandi, *Biosens. Bioelectron.* **2016**, *81*, 465.
3. S. Tao, T. Feng, C. Zheng, S. Zhu, B. Yang, *J. Phys. Chem. Lett.* **2019**, *10*, 5182.
4. a) K. Nekouei, M. Amiri, M. Sillanpää, F. Marken, R. Boukherroub, S. Szunerits, *Chem. Soc. Rev.* **2019**, *48*, 4281; b) M. Han, S. Zhu, S. Lu, Y. Song, T. Feng, S. Tao, J. Liu, B. Yang, *Nano Today* **2018**, *19*, 201.
5. K. J. Mintz, Y. Zhou, R. M. Leblanc, *Nanoscale* **2019**, *11*, 4634.
6. K. Jiang, Y. Wang, C. Cai, H. Lin, *Chem. Mater.* **2017**, *29*, 4866.
7. M. J. Sweetman, S. M. Hickey, D. A. Brooks, J. D. Hayball, S. E. Plush, *Adv. Funct. Mater.* **2019**, *29*, 1808740.
8. A. M. Schwenke, S. Hoeppener, U. S. Schubert, *Adv. Mater.* **2015**, *27*, 4113.
9. S. Y. Lim, W. Shen, Z. Gao, *Chem. Soc. Rev.* **2015**, *44*, 362.
10. Y. Du, S. Guo, *Nanoscale* **2016**, *8*, 2532.
11. Y. Xu, J. Liu, C. Gao, E. Wang, *Electrochem. Commun.* **2014**, *48*, 151.
12. a) K. I. Bolotin, K. J. Sikes, Z. Jiang, M. Klima, G. Fudenberg, J. Hone, P. Kim, H. L. Stormer, *Solid State Commun.* **2008**, *146*, 351; b) L. A. Ponomarenko, F. Schedin, M. I. Katsnelson, R. Yang, E. W. Hill, K. S. Novoselov, A. K. Geim, *Science* **2008**, *320*, 356.
13. S. Zhu, Y. Song, X. Zhao, J. Shao, J. Zhang, B. Yang, *Nano Res.* **2015**, *8*, 355.
14. H. A. Nguyen, I. Srivastava, D. Pan, M. Gruebele, *ACS Nano* **2020**, *14*, 6127–6137.
15. N. V. Teplakov, E. V. Kundele, P. D. Khavlyuk, Y. Xiong, M. Y. Leonov, W. Zhu, A. V. Baranov, A. V. Fedorov, A. L. Rogach, I. D. Rukhlenko, *ACS Nano* **2019**, *13*, 10737.
16. R. Liu, D. Wu, X. Feng, K. Müllen, *J. Am. Chem. Soc.* **2011**, *133*, 15221.
17. J. Zhou, C. Booker, R. Li, X. Zhou, T. K. Sham, X. Sun, Z. Ding, *J. Am. Chem. Soc.* **2007**, *129*, 744.
18. F. Wang, Z. Xie, H. Zhang, C.-Y. Liu, Y.-G. Zhang, *Adv. Funct. Mater.* **2011**, *21*, 1027.
19. M. Zheng, S. Liu, J. Li, D. Qu, H. Zhao, X. Guan, X. Hu, Z. Xie, X. Jing, Z. Sun, *Adv. Mater.* **2014**, *26*, 3554.
20. L. Li, G. Wu, G. Yang, J. Peng, J. Zhao, J.-J. Zhu, *Nanoscale* **2013**, *5*, 4015.
21. S. Zhu, J. Zhang, S. Tang, C. Qiao, L. Wang, H. Wang, X. Liu, B. Li, Y. Li, W. Yu, X. Wang, H. Sun, B. Yang, *Adv. Funct. Mater.* **2012**, *22*, 4732.
22. M. Zhang, L. Bai, W. Shang, W. Xie, H. Ma, Y. Fu, D. Fang, H. Sun, L. Fan, M. Han, C. Liu, S. Yang, *J. Mater. Chem.* **2012**, *22*, 7461.
23. M. Li, C. Hu, C. Yu, S. Wang, P. Zhang, J. Qiu, *Carbon* **2015**, *91*, 291.
24. S. Qu, D. Zhou, D. Li, W. Ji, P. Jing, D. Han, L. Liu, H. Zeng, D. Shen, *Adv. Mater.* **2016**, *28*, 3516.
25. I. Srivastava, S. K. Misra, I. Tripathi, A. Schwartz-Duval, D. Pan, *Adv. Biosyst.* **2018**, *2*, 1800009.
26. P. Fathi, J. S. Khamo, X. Huang, I. Srivastava, M. B. Esch, K. Zhang, D. Pan, *Carbon* **2019**, *145*, 572.
27. S. Do, W. Kwon, Y.-H. Kim, S. R. Kang, T. Lee, T.-W. Lee, S.-W. Rhee, *Adv. Opt. Mater.* **2016**, *4*, 276.
28. W. Tang, Y. Wang, P. Wang, J. Di, J. Yang, Y. Wu, *Microchim. Acta* **2016**, *183*, 2571.
29. a) X. Wang, L. Cao, S. T. Yang, F. Lu, M. J. Mezziani, L. Tian, K. W. Sun, M. A. Bloodgood, Y. P. Sun, *Angew. Chem., Int. Ed. Engl.* **2010**, *49*, 5310; b) H. Tetsuka, R. Asahi, A. Nagoya, K. Okamoto, I. Tajima, R. Ohta, A. Okamoto, *Adv. Mater.* **2012**, *24*, 5333.
30. J. Shi, C. Chan, Y. Pang, W. Ye, F. Tian, J. Lyu, Y. Zhang, M. Yang, *Biosens. Bioelectron.* **2015**, *67*, 595.
31. S. P. Jovanović, Z. Syrgiannis, M. D. Budimir, D. D. Milivojević, D. J. Jovanovic, V. B. Pavlović, J. M. Papan, M. Bartenwerfer, M. M. Mojsin, M. J. Stevanović, B. M. Todorović Marković, *Mater. Sci. Eng. C* **2020**, *109*, 110539.
32. C. S. Lim, K. Hla, A. Ambrosi, R. Zboril, M. Pumera, *Electrochem. Commun.* **2015**, *52*, 75.
33. J. Liu, R. Li, B. Yang, *ACS Central Sci.* **2020**, *6*, 2179.
34. M. L. Yola, N. Atar, *J. Electrochem. Soc.* **2018**, *165*, H1.
35. B. D. Mansuriya, Z. Altintas, *Sensors (Basel)* **2020**, *20*, 1072.
36. H. Rao, X. Zhao, X. Liu, J. Zhong, Z. Zhang, P. Zou, Y. Jiang, X. Wang, Y. Wang, *Biosens. Bioelectron.* **2018**, *100*, 341.
37. B. Demir, M. M. Lemberger, M. Panagiotopoulou, P. X. Medina Rangel, S. Timur, T. Hirsch, B. Tse Sum Bui, J. Wegener, K. Haupt, *ACS Appl. Mater. Interfaces* **2018**, *10*, 3305.
38. D. Iannazzo, A. Pistone, M. Salamò, S. Galvagno, R. Romeo, S. V. Giofrè, C. Branca, G. Visalli, A. Di Pietro, *Int. J. Pharm.* **2017**, *518*, 185.
39. C. J. Reckmeier, Y. Wang, R. Zboril, A. L. Rogach, *J. Phys. Chem. C* **2016**, *120*, 10591.
40. X. Ren, F. Zhang, B. Guo, N. Gao, X. Zhang, *Nanomaterials (Basel)* **2019**, *9*, 495.
41. D. Qu, M. Zheng, L. Zhang, H. Zhao, Z. Xie, X. Jing, R. E. Hadad, H. Fan, Z. Sun, *Sci. Rep.* **2014**, *4*, 5294.
42. F. A. Permatasari, A. H. Aimon, F. Iskandar, T. Ogi, K. Okuyama, *Sci. Rep.* **2016**, *6*, 21042.
43. a) M. Lu, L. Zhou, *Mater. Sci. Eng. C Mater. Biol. Appl.* **2019**, *101*, 352; b) P. Ray, E. Xu, V. H. Crespi, J. V. Badding, A. D. Lueking, *PCCP* **2018**, *20*, 15411.
44. P. Ray, D. Gidley, J. V. Badding, A. D. Lueking, *Microporous Mesoporous Mater.* **2019**, *277*, 29.
45. X. Niu, Y. Li, H. Shu, J. Wang, *Nanoscale* **2016**, *8*, 19376.
46. W. Yang, H. Zhang, J. Lai, X. Peng, Y. Hu, W. Gu, L. Ye, *Carbon* **2018**, *128*, 78.

47. T.-F. Yeh, C.-Y. Teng, S.-J. Chen, H. Teng, *Adv. Mater.* **2014**, *26*, 3297.
48. Q. Zhang, S. Xie, Y. Yang, Y. Wu, X. Wang, J. Wu, L. Zhang, J. Chen, Y. Wang, *J. Anal. Methods Chem.* **2018**, *2018*, 7890937.
49. I. Srivastava, J. S. Khamo, S. Pandit, P. Fathi, X. Huang, A. Cao, R. T. Haasch, S. Nie, K. Zhang, D. Pan, *Adv. Funct. Mater.* **2019**, *29*, 1902466.
50. P. Moitra, M. Alafeef, K. Dighe, M. B. Frieman, D. Pan, *ACS Nano* **2020**, *14*, 7617.
51. F. Li, C. Liu, J. Yang, Z. Wang, W. Liu, F. Tian, *RSC Adv.* **2014**, *4*, 3201.
52. N. Parvin, T. K. Mandal, *Microchim. Acta* **2017**, *184*, 1117.
53. D. Sun, R. Ban, P.-H. Zhang, G.-H. Wu, J.-R. Zhang, J.-J. Zhu, *Carbon* **2013**, *64*, 424.
54. S. C. Ray, A. Saha, N. R. Jana, R. Sarkar, *J. Phys. Chem. C* **2009**, *113*, 18546.
55. J. Peng, W. Gao, B. K. Gupta, Z. Liu, R. Romero-Aburto, L. Ge, L. Song, L. B. Alemany, X. Zhan, G. Gao, S. A. Vithayathil, B. A. Kaiparettu, A. A. Marti, T. Hayashi, J. J. Zhu, P. M. Ajayan, *Nano Lett.* **2012**, *12*, 844.
56. W. Shang, X. Zhang, M. Zhang, Z. Fan, Y. Sun, M. Han, L. Fan, *Nanoscale* **2014**, *6*, 5799.
57. S. K. Misra, I. Srivastava, I. Tripathi, E. Daza, F. Ostadhossein, D. Pan, *J. Am. Chem. Soc.* **2017**, *139*, 1746.
58. R. Zhang, Y. Liu, L. Yu, Z. Li, S. Sun, *Nanotechnology* **2013**, *24*, 225601.
59. S. N. Baker, G. A. Baker, *Angew. Chem., Int. Ed.* **2010**, *49*, 6726.
60. X. Huang, F. Zhang, L. Zhu, K. Y. Choi, N. Guo, J. Guo, K. Tackett, P. Anilkumar, G. Liu, Q. Quan, H. S. Choi, G. Niu, Y.-P. Sun, S. Lee, X. Chen, *ACS Nano* **2013**, *7*, 5684.
61. N. Abdullah Al, J.-E. Lee, I. In, H. Lee, K. D. Lee, J. H. Jeong, S. Y. Park, *Mol. Pharm.* **2013**, *10*, 3736.
62. I. Srivastava, D. Sar, P. Mukherjee, A. S. Schwartz-Duval, Z. Huang, C. Jaramillo, A. Civantos, I. Tripathi, J. P. Allain, R. Bhargava, D. Pan, *Nanoscale* **2019**, *11*, 8226.
63. V. Mishra, A. Patil, S. Thakur, P. Kesharwani, *Drug Discov. Today* **2018**, *23*, 1219.
64. a) S. K. Misra, I. Srivastava, J. S. Khamo, V. V. Krishnamurthy, D. Sar, A. S. Schwartz-Duval, J. A. N. T. Soares, K. Zhang, D. Pan, *Nanoscale* **2018**, *10*, 18510; b) H. Zhu, X. Wang, Y. Li, Z. Wang, F. Yang, X. Yang, *Chem. Commun.* **2009**, 5118.
65. H. Li, X. He, Y. Liu, H. Huang, S. Lian, S.-T. Lee, Z. Kang, *Carbon* **2011**, *49*, 605.
66. H. Liu, T. Ye, C. Mao, *Angew. Chem., Int. Ed.* **2007**, *46*, 6473.
67. L. Wu, X. Cai, K. Nelson, W. Xing, J. Xia, R. Zhang, A. J. Stacy, M. Luderer, G. M. Lanza, L. V. Wang, B. Shen, D. Pan, *Nano Res.* **2013**, *6*, 312.
68. a) P. G. Kuzmin, G. A. Shafeev, V. V. Bukin, S. V. Garnov, C. Farcau, R. Carles, R. Warot-Fontrose, V. Guieu, G. Viau, *J. Phys. Chem. C* **2010**, *114*, 15266; b) C. Doñate-Buendia, R. Torres-Mendieta, A. Pyatenko, E. Falomir, M. Fernández-Alonso, G. Mínguez-Vega, *ACS Omega* **2018**, *3*, 2735; c) C.-Y. Wang, P. Ray, Q. Gong, Y. Zhao, J. Li, A. D. Lueking, *PCCP* **2015**, *17*, 26766.
69. M. S. Ghamsari, *State of the Art in Nano-bioimaging*, BoD—Books on Demand, **2018**.
70. S.-L. Hu, K.-Y. Niu, J. Sun, J. Yang, N.-Q. Zhao, X.-W. Du, *J. Mater. Chem.* **2009**, *19*, 484.
71. Y. P. Sun, B. Zhou, Y. Lin, W. Wang, K. A. Fernando, P. Pathak, M. J. Mezziani, B. A. Harruff, X. Wang, H. Wang, P. G. Luo, H. Yang, M. E. Kose, B. Chen, L. M. Veca, S. Y. Xie, *J. Am. Chem. Soc.* **2006**, *128*, 7756.
72. X. Li, H. Wang, Y. Shimizu, A. Pyatenko, K. Kawaguchi, N. Koshizaki, *Chem. Commun.* **2011**, *47*, 932.
73. J. Deng, Q. Lu, N. Mi, H. Li, M. Liu, M. Xu, L. Tan, Q. Xie, Y. Zhang, S. Yao, *Chem. – Eur. J.* **2014**, *20*, 4993.
74. Y. Hou, Q. Lu, J. Deng, H. Li, Y. Zhang, *Anal. Chim. Acta* **2015**, *866*, 69.
75. T. Xing, J. Sunarso, W. Yang, Y. Yin, A. M. Glushenkov, L. H. Li, P. C. Howlett, Y. Chen, *Nanoscale* **2013**, *5*, 7970.
76. O. V. Kharissova, B. I. Kharisov, C. M. Oliva González, Y. P. Méndez, I. López, *R. Soc. Open Sci.*, *6*, 191378.
77. S. L. James, C. J. Adams, C. Bolm, D. Braga, P. Collier, T. Friščić, F. Grepioni, K. D. M. Harris, G. Hyett, W. Jones, A. Krebs, J. Mack, L. Maini, A. G. Orpen, I. P. Parkin, W. C. Shearouse, J. W. Steed, D. C. Waddell, *Chem. Soc. Rev.* **2012**, *41*, 413.
78. X. H. Chen, H. S. Yang, G. T. Wu, M. Wang, F. M. Deng, X. B. Zhang, J. C. Peng, W. Z. Li, *J. Cryst. Growth* **2000**, *218*, 57.
79. H. Li, X. He, Y. Liu, H. Yu, Z. Kang, S.-T. Lee, *Mater. Res. Bull.* **2011**, *46*, 147.
80. H. Dang, L.-K. Huang, Y. Zhang, C.-F. Wang, S. Chen, *Ind. Eng. Chem. Res.* **2016**, *55*, 5335.
81. F. Wang, S. Wang, Z. Sun, H. Zhu, *Fullerenes, Nanotubes Carbon Nanostr.* **2015**, *23*, 769.
82. Q. Liu, N. Zhang, H. Shi, W. Ji, X. Guo, W. Yuan, Q. Hu, *New J. Chem.* **2018**, *42*, 3097.
83. Z. Zhu, P. Yang, M. Chen, T. Zhang, Y. Cao, W. Zhang, X. Zhou, W. Chen, *J. Lumin.* **2019**, *213*, 474.
84. S. Sahu, B. Behera, T. K. Maiti, S. Mohapatra, *Chem. Commun.* **2012**, *48*, 8835.
85. a) X. Yang, Y. Zhuo, S. Zhu, Y. Luo, Y. Feng, Y. Dou, *Biosens. Bioelectron.* **2014**, *60*, 292; b) L. Wu, X. Cai, K. Nelson, W. Xing, J. Xia, R. Zhang, A. J. Stacy, M. Luderer, G. M. Lanza, L. V. Wang, B. Shen, D. Pan, *Nano Res* **2013**, *6*, 312.
86. P.-C. Hsu, H.-T. Chang, *Chem. Commun.* **2012**, *48*, 3984.
87. S. Zhu, Q. Meng, L. Wang, J. Zhang, Y. Song, H. Jin, K. Zhang, H. Sun, H. Wang, B. Yang, *Angew. Chem., Int. Ed. Engl.* **2013**, *52*, 3953.
88. L. Lin, Y. Wang, Y. Xiao, W. Liu, *Microchim. Acta* **2019**, *186*, 147.
89. Z. Qian, X. Shan, L. Chai, J. Ma, J. Chen, H. Feng, *ACS Appl. Mater. Interfaces* **2014**, *6*, 6797.
90. Y.-Q. Zhang, D.-K. Ma, Y. Zhuang, X. Zhang, W. Chen, L.-L. Hong, Q.-X. Yan, K. Yu, S.-M. Huang, *J. Mater. Chem.* **2012**, *22*, 16714.
91. X. Shan, L. Chai, J. Ma, Z. Qian, J. Chen, H. Feng, *Analyst* **2014**, *139*, 2322.
92. A. B. Bourlinos, G. Trivizas, M. A. Karakassides, M. Baikousi, A. Kouloumpis, D. Gournis, A. Bakandritsos, K. Hala, O. Kozak, R. Zboril, I. Papagiannouli, P. Aloukos, S. Couris, *Carbon* **2015**, *83*, 173.
93. T. Feng, X. Ai, G. An, P. Yang, Y. Zhao, *ACS Nano* **2016**, *10*, 4410.
94. M. Zheng, S. Ruan, S. Liu, T. Sun, D. Qu, H. Zhao, Z. Xie, H. Gao, X. Jing, Z. Sun, *ACS Nano* **2015**, *9*, 11455.
95. N. Akakura, M. Kobayashi, I. Horiuchi, A. Suzuki, J. Wang, J. Chen, H. Niizeki, K. Kawamura, M. Hosokawa, M. Asaka, *Cancer Res.* **2001**, *61*, 6548.
96. F. Wang, S. Pang, L. Wang, Q. Li, M. Kreiter, C.-Y. Liu, *Chem. Mater.* **2010**, *22*, 4528.

97. L. Wu, M. Luderer, X. Yang, C. Swain, H. Zhang, K. Nelson, A. J. Stacy, B. Shen, G. M. Lanza, D. Pan, *Theranostics* **2013**, 3, 677.
98. L. Zheng, Y. Chi, Y. Dong, J. Lin, B. Wang, *J. Am. Chem. Soc.* **2009**, 131, 4564.
99. O. S. Wolfbeis, *Chem. Soc. Rev.* **2015**, 44, 4743.
100. F. Ostadhossein, S. K. Misra, P. Mukherjee, A. Ostadhossein, E. Daza, S. Tiwari, S. Mittal, M. C. Gryka, R. Bhargava, D. Pan, *Small* **2016**, 12, 5845.
101. P. Zuo, X. Lu, Z. Sun, Y. Guo, H. He, *Microchim. Acta* **2016**, 183, 519.
102. A. Zhu, Q. Qu, X. Shao, B. Kong, Y. Tian, *Angew. Chem., Int. Ed.* **2012**, 51, 7185.
103. F. Ostadhossein, G. Vulugundam, S. K. Misra, I. Srivastava, D. Pan, *Bioconjug. Chem.* **2018**, 29, 3913.
104. G. Vulugundam, S. K. Misra, F. Ostadhossein, A. S. Schwartz-Duval, E. A. Daza, D. Pan, *Chem. Commun.* **2016**, 52, 7513.
105. I. Tripathi, S. K. Misra, F. Ostadhossein, I. Srivastava, D. Pan, *ACS Appl. Mater. Interfaces* **2018**, 10, 37886.
106. a) C. Xia, S. Zhu, T. Feng, M. Yang, B. Yang, *Adv. Sci.* **2019**, 6, 1901316; b) H. Ding, S.-B. Yu, J.-S. Wei, H.-M. Xiong, *ACS Nano* **2016**, 10, 484.
107. C. Xia, S. Tao, S. Zhu, Y. Song, T. Feng, Q. Zeng, J. Liu, B. Yang, *Chem. – Eur. J.* **2018**, 24, 11303.
108. J. K. Ray, S. Paul, P. Ray, R. Singha, D. Y. Rao, S. Nandi, A. Anoop, *New J. Chem.* **2017**, 41, 278.
109. S. Chaudhuri, S. Maity, M. Roy, P. Ray, J. K. Ray, *Asian J. Chem.* **2016**, 28.
110. S. Zhu, L. Wang, N. Zhou, X. Zhao, Y. Song, S. Maharjan, J. Zhang, L. Lu, H. Wang, B. Yang, *Chem. Commun.* **2014**, 50, 13845.
111. Y. Song, S. Zhu, J. Shao, B. Yang, *J. Polym. Sci., Part A Polym. Chem.* **2017**, 55, 610.
112. S. Lu, L. Sui, J. Liu, S. Zhu, A. Chen, M. Jin, B. Yang, *Adv. Mater.* **2017**, 29, 1603443.
113. a) S. Tao, S. Zhu, T. Feng, C. Xia, Y. Song, B. Yang, *Mater. Today Chem.* **2017**, 6, 13; b) S. Tao, Y. Song, S. Zhu, J. Shao, B. Yang, *Polymer* **2017**, 116, 472.
114. V. Nguyen, L. Yan, J. Si, X. Hou, *J. Appl. Phys.* **2015**, 117, 084304.
115. H. Yu, X. Li, X. Zeng, Y. Lu, *Chem. Commun.* **2016**, 52, 819.
116. T. Xing, J. Sunarso, W. Yang, Y. Yin, A. M. Glushenkov, L. H. Li, P. C. Howlett, Y. Chen, *Nanoscale* **2013**, 5, 7970.
117. Y. Han, Y. Chen, N. Wang, Z. He, *Mater. Technol.* **2019**, 34, 336.
118. Z. Ma, H. Ming, H. Huang, Y. Liu, Z. Kang, *New J. Chem.* **2012**, 36, 861.
119. C. Liu, P. Zhang, X. Zhai, F. Tian, W. Li, J. Yang, Y. Liu, H. Wang, W. Wang, W. Liu, *Biomaterials* **2012**, 33, 3604.
120. C. H. Lei, X. E. Zhao, S. L. Jiao, L. He, Y. Li, S. Y. Zhu, J. M. You, *Anal. Methods* **2016**, 8, 4438.
121. X. Cao, J. Wang, W. Deng, J. Chen, Y. Wang, J. Zhou, P. Du, W. Xu, Q. Wang, Q. Wang, Q. Yu, M. Spector, J. Yu, X. Xu, *Sci. Rep.* **2018**, 8, 7057.
122. J. Zhou, Z. Sheng, H. Han, M. Zou, C. Li, *Mater. Lett.* **2012**, 66, 222.
123. J. Song, L. Zhao, Y. Wang, Y. Xue, Y. Deng, X. Zhao, Q. Li, *Nanomaterials* **2018**, 8, 1043.
124. N. Vasimalai, V. Vilas-Boas, J. Gallo, M. D. F. Cerqueira, M. Menéndez-Miranda, J. M. Costa-Fernández, L. Diéguez, B. Espiña, M. T. Fernández-Argüelles, *Beilstein J. Nanotechnol.* **2018**, 9, 530.
125. H. Yang, Y. Liu, Z. Guo, B. Lei, J. Zhuang, X. Zhang, Z. Liu, C. Hu, *Nat. Commun.* **2019**, 10, 1789.
126. S. Zhu, J. Zhang, L. Wang, Y. Song, G. Zhang, H. Wang, B. Yang, *Chem. Commun.* **2012**, 48, 10889.
127. V. Georgakilas, J. A. Perman, J. Tucek, R. Zboril, *Chem. Rev.* **2015**, 115, 4744.
128. F. Ostadhossein, D. Pan, *WIREs Nanomed. Nanobiotechnol.* **2017**, 9, e1436.
129. X. Zhai, P. Zhang, C. Liu, T. Bai, W. Li, L. Dai, W. Liu, *Chem. Commun.* **2012**, 48, 7955.
130. A. Kasouni, T. Chatzimitakos, C. Stalikas, *J. Carbon Res.* **2019**, 5, 19.
131. F. Ostadhossein, L. Benig, I. Tripathi, S. K. Misra, D. Pan, *ACS Appl. Mater. Interfaces* **2018**, 10, 19408.
132. V. N. Mehta, S. Jha, R. K. Singhal, S. K. Kailasa, *New J. Chem.* **2014**, 38, 6152.
133. H. A. Nguyen, I. Srivastava, D. Pan, M. Gruebele, *Proc. Nat. Acad. Sci.* **2021**, 118, e2023083118.
134. H. Tao, K. Yang, Z. Ma, J. Wan, Y. Zhang, Z. Kang, Z. Liu, *Small* **2012**, 8, 281.
135. P. Ray, L. Alhalhooly, A. Ghosh, Y. Choi, S. Banerjee, S. Mallik, S. Banerjee, M. Quadir, *ACS Biomater. Sci. Eng.* **2019**, 5, 1354.
136. S.-T. Yang, L. Cao, P. G. Luo, F. Lu, X. Wang, H. Wang, M. J. Mezziani, Y. Liu, G. Qi, Y.-P. Sun, *J. Am. Chem. Soc.* **2009**, 131, 11308.
137. H. Gong, R. Peng, Z. Liu, *Adv. Drug. Deliv. Rev.* **2013**, 65, 1951.
138. Y. Zhang, M. Wu, M. Wu, J. Zhu, X. Zhang, *ACS Omega* **2018**, 3, 9126.
139. H. Chen, Z. Wang, S. Zong, L. Wu, P. Chen, D. Zhu, C. Wang, S. Xu, Y. Cui, *ACS Appl. Mater. Interfaces* **2014**, 6, 17526.
140. H. Li, Z. Kang, Y. Liu, S.-T. Lee, *J. Mater. Chem.* **2012**, 22, 24230.
141. P. Mukherjee, S. K. Misra, M. C. Gryka, H.-H. Chang, S. Tiwari, W. L. Wilson, J. W. Scott, R. Bhargava, D. Pan, *Small* **2015**, 11, 4691.
142. Z. Liu, S. Tabakman, K. Welscher, H. Dai, *Nano Res.* **2009**, 2, 85.
143. D. Roxbury, P. V. Jena, R. M. Williams, B. Enyedi, P. Niethammer, S. Marcet, M. Verhaegen, S. Blais-Ouellette, D. A. Heller, *Sci. Rep.* **2015**, 5, 14167.
144. S. K. Misra, F. Ostadhossein, E. Daza, E. V. Johnson, D. Pan, *Adv. Funct. Mater.* **2016**, 26, 8031.
145. J. Zhang, S.-H. Yu, *Mater. Today* **2016**, 19, 382.
146. H. Wang, R. Revia, K. Wang, R. J. Kant, Q. Mu, Z. Gai, K. Hong, M. Zhang, *Adv. Mater.* **2017**, 29.
147. H. Chen, G. D. Wang, W. Tang, T. Todd, Z. Zhen, C. Tsang, K. Hekmatyar, T. Cowger, R. B. Hubbard, W. Zhang, J. Stickney, B. Shen, J. Xie, *Adv. Mater.* **2014**, 26, 6761.
148. Y. Xu, X.-H. Jia, X.-B. Yin, X.-W. He, Y.-K. Zhang, *Anal. Chem.* **2014**, 86, 12122.
149. Y. Wang, T. Wang, X. Chen, Y. Xu, H. Li, *Opt. Mater.* **2018**, 78, 118.
150. P. Beard, *Interface Focus* **2011**, 1, 602.
151. D. Pan, B. Kim, L. V. Wang, G. M. Lanza, *WIREs Nanomed. Nanobiotechnol.* **2013**, 5, 517.
152. L. Wang, Y. Yin, A. Jain, H. S. Zhou, *Langmuir* **2014**, 30, 14270.
153. J. Tang, B. Kong, H. Wu, M. Xu, Y. Wang, D. Zhao, G. Zheng, *Adv. Mater.* **2013**, 25, 6569.
154. H. Wang, J. Di, Y. Sun, J. Fu, Z. Wei, H. Matsui, A. del C. Alonso, S. Zhou, *Adv. Funct. Mater.* **2015**, 25, 5537.



155. S. K. Bhunia, L. Zeiri, J. Manna, S. Nandi, R. Jelinek, *ACS Appl. Mater. Interfaces* **2016**, *8*, 25637.
156. J. Ge, Q. Jia, W. Liu, L. Guo, Q. Liu, M. Lan, H. Zhang, X. Meng, P. Wang, *Adv. Mater.* **2015**, *27*, 4169.
157. Q. Jia, X. Zheng, J. Ge, W. Liu, H. Ren, S. Chen, Y. Wen, H. Zhang, J. Wu, P. Wang, *J. Colloid Interface Sci.* **2018**, *526*, 302.
158. X. Bao, Y. Yuan, J. Chen, B. Zhang, D. Li, D. Zhou, P. Jing, G. Xu, Y. Wang, K. Holá, D. Shen, C. Wu, L. Song, C. Liu, R. Zbořil, S. Qu, *Light: Sci. Appl.* **2018**, *7*, 91.
159. H. Tao, K. Yang, Z. Ma, J. Wan, Y. Zhang, Z. Kang, Z. Liu, *Small* **2012**, *8*, 281.
160. a) V. S. Sivasankarapillai, A. V. Kirthi, M. Akksadha, S. Indu, U. D. Dharshini, J. Pushpamalar, L. Karthik, *Nanoscale Adv.* **2020**, *2*, 1760; b) M. Alafeef, K. Dighe, P. Moitra, D. Pan, *ACS Nano* **2020**, *14*, 17028; c) M. Alafeef, P. Moitra, D. Pan, *Biosens. Bioelectron.* **2020**, *165*, 112276; d) I. Srivastava, M. S. Khan, K. Dighe, M. Alafeef, Z. Wang, T. Banerjee, T. Ghonge, L. M. Grove, R. Bashir, D. Pan, *Small Methods* **2020**, *4*, 2070022; e) I. Srivastava, S. K. Misra, S. Bangru, K. A. Boateng, J. A. N. T. Soares, A. S. Schwartz-Duval, A. Kalsotra, D. Pan, *ACS Appl. Mater. Interfaces* **2020**, *12*, 16137; f) M. Alafeef, K. Dighe, D. Pan, *ACS Appl. Mater. Interfaces* **2019**, *11*, 42943; g) S. K. Misra, K. Dighe, A. S. Schwartz-Duval, Z. Shang, L. T. Labriola, D. Pan, *Biosens. Bioelectron.* **2018**, *120*, 77; h) P. Moitra, D. Bhagat, V. B. Kamble, A. M. Umarji, R. Pratap, S. Bhattacharya, *Biosens. Bioelectron.* **2021**, *173*, 112728; i) M. S. Khan, S. K. Misra, Z. Wang, E. Daza, A. S. Schwartz-Duval, J. M. Kus, D. Pan, D. Pan, *Anal. Chem.* **2017**, *89*, 2107; j) P. Moitra, M. Alafeef, K. Dighe, P. Ray, J. Chang, S. S. Ramamurthy, X. Ge, D. Pan, G. Rao, *medRxiv* **2020**, 2020.10.08.20208785; k) J. K. Ray, R. Singha, D. Ray, P. Ray, D. Y. Rao, A. Anoop, *Tetrahedron Lett.* **2019**, *60*, 931.
161. Y. Wang, A. Hu, *J. Mater. Chem. C* **2014**, *2*, 6921.
162. X. Wu, F. Tian, W. Wang, J. Chen, M. Wu, J. X. Zhao, *J. Mater. Chem. C Mater.* **2013**, *1*, 4676.
163. P. K. Jain, X. Huang, I. H. El-Sayed, M. A. El-Sayed, *Plasmonics* **2007**, *2*, 107.
164. a) P. Ray, M. Clément, C. Martini, I. Abdellah, P. Beaunier, J.-L. Rodriguez-Lopez, V. Huc, H. Remita, I. Lampre, *New J. Chem.* **2018**, *42*, 14128; b) M. Clément, I. Abdellah, P. Ray, C. Martini, Y. Coppel, H. Remita, I. Lampre, V. Huc, *Inorg. Chem. Front.* **2020**, *7*, 953; c) E. André, B. Boutonnet, P. Charles, C. Martini, J.-M. Aguiar-Hualde, S. Latil, V. Guérineau, K. Hammad, P. Ray, R. Guillot, V. Huc, *Chem. Eur. J.* **2016**, *22*, 3105; d) P. K. Jain, M. A. El-Sayed, *Nano Lett.* **2008**, *8*, 4347.
165. a) D. Yoo, Y. Park, B. Cheon, M.-H. Park, *Nanoscale Res. Lett.* **2019**, *14*, 272; b) A. Sharma, J. Das, *J. Nanobiotechnol.* **2019**, *17*, 92; c) M. Zhang, R. Su, J. Zhong, L. Fei, W. Cai, Q. Guan, W. Li, N. Li, Y. Chen, L. Cai, Q. Xu, *Nano Res.* **2019**, *12*, 815; d) H. Li, X. Yan, S. Qiao, G. Lu, X. Su, *ACS Appl. Mater. Interfaces* **2018**, *10*, 7737; (e) E. A. Daza, S. K. Misra, J. Scott, I. Tripathi, C. Promisel, B. K. Sharma, J. Topczewski, S. Chaudhuri, D. Pan, *Sci. Rep.* **2017**, *7*, 41880; (f) S. Brahma, P. Ray, R. Singha, J. K. Ray, *Asian J. Chem.* **2016**, *28*, 1035; (g) R. Singha, S. Roy, S. Nandi, P. Ray, J. K. Ray, *Tetrahedron Lett.* **2013**, *54*, 657; (h) D. Ray, Y. Nasima, M. K. Sajal, P. Ray, S. Urinda, A. Anoop, J. K. Ray, *Synthesis* **2013**, *45*, 1261.
166. I. Tripathi, L. K. Dodgen, F. Ostadhossein, S. K. Misra, E. Daza, B. K. Sharma, W. Zheng, D. Pan, *J. Mat. Chem. A* **2018**, *6*, 22951.
167. S. Pandit, T. Banerjee, I. Srivastava, S. Nie, D. Pan, *ACS Sensors* **2019**, *4*, 2730.
168. R. Franco, J. A. Cidowski, *Cell Death Differ.* **2009**, *16*, 1303.
169. G. K. Balendiran, R. Dabur, D. Fraser, *Cell Biochem. Funct.* **2004**, *22*, 343.
170. P. T. Lee, D. Lowinsohn, R. G. Compton, *Electroanalysis* **2014**, *26*, 1488.
171. a) S. Karthik, B. Saha, S. K. Ghosh, N. D. Pradeep Singh, *Chem. Commun.* **2013**, *49*, 10471; b) V. Kumar, G. Toffoli, F. Rizzolio, *ACS Med. Chem. Lett.* **2013**, *4*, 1012; c) E. A. Daza, A. S. Schwartz-Duval, K. Volkman, D. Pan, *ACS Biomater. Sci. Eng.* **2018**, *4*, 1357; d) T. Kampert, S. K. Misra, I. Srivastava, I. Tripathi, D. Pan, *Cell Mol. Bioeng.* **2017**, *10*, 371; e) S. K. Misra, F. Ostadhossein, R. Babu, J. Kus, D. Tankasala, A. Sutrisno, K. A. Walsh, C. R. Bromfield, D. Pan, *Adv Healthcare Mater.* **2017**, *6*, 1700008.
172. a) T. A. Ahmed, B. M. Aljaeid, *Drug Des. Devel. Ther.* **2016**, *10*, 483; b) R. Bhattacharya, P. Mukherjee, *Adv. Drug. Deliv. Rev.* **2008**, *60*, 1289; c) P. Cherukuri, E. S. Glazer, S. A. Curley, *Adv. Drug. Deliv. Rev.* **2010**, *62*, 339; d) B. C. Patra, S. K. Das, A. Ghosh, A. Raj K, P. Moitra, M. Addicoat, S. Mitra, A. Bhaumik, S. Bhattacharya, A. Pradhan, *Jo. Mater. Chem. A* **2018**, *6*, 16655; e) N. C. Sarker, P. Ray, C. Pfau, V. Kalavacharla, K. Hossain, M. Quadir, *J. Agric. Food Chem.* **2020**, *68*, 4367.
173. a) P. Ray, M. Ferraro, R. Haag, M. Quadir, *Macromol. Biosci.* **2019**, *19*, e1900073; b) S. Mitragotri, D. G. Anderson, X. Chen, E. K. Chow, D. Ho, A. V. Kabanov, J. M. Karp, K. Kataoka, C. A. Mirkin, S. H. Petrosko, J. Shi, M. M. Stevens, S. Sun, S. Teoh, S. S. Venkatraman, Y. Xia, S. Wang, Z. Gu, C. Xu, *ACS Nano* **2015**, *9*, 6644; c) P. Ray, G. Nair, A. Ghosh, S. Banerjee, M. Y. Golovko, S. K. Banerjee, K. M. Reindl, S. Mallik, M. Quadir, *J. Cell Commun. Signal.* **2019**, *13*, 407–420. d) C. S. Abdullah, P. Ray, S. Alam, N. Kale, R. Aishwarya, M. Morshed, D. Dutta, C. Hudziak, S. K. Banerjee, S. Mallik, S. Banerjee, M. S. Bhuiyan, M. Quadir, *Mol. Pharm.* **2020**, *17*, 4676–4690. e) P. Ray, M. Confeld, P. Borowicz, T. Wang, S. Mallik, M. Quadir, *Colloids Surf. B* **2019**, *174*, 126; f) P. Ray, D. Dutta, I. Haque, G. Nair, J. Mohammed, M. Parmer, N. Kale, M. Orr, P. Jain, S. Banerjee, K. M. Reindl, S. Mallik, S. Kambhampati, S. K. Banerjee, M. Quadir, *Mol. Pharm.* **2020**, *18*, 87–100. g) P. Ray, N. Kale, M. Quadir, *Colloids Surf. B* **2021**, *200*, 111563; h) M. I. Confeld, B. Mamnoon, L. Feng, H. Jensen-Smith, P. Ray, J. Froberg, J. Kim, M. A. Hollingsworth, M. Quadir, Y. Choi, S. Mallik, *Mol. Pharm.* **2020**, *17*, 2849.
174. D. Pan, J. L. Turner, K. L. Wooley, *Chem. Commun.* **2003**, 2400.
175. a) D. Pan, S. D. Caruthers, G. Hu, A. Senpan, M. J. Scott, P. J. Gaffney, S. A. Wickline, G. M. Lanza, *J. Am. Chem. Soc.* **2008**, *130*, 9186; b) D. Pan, G. M. Lanza, S. A. Wickline, S. D. Caruthers, *Eur. J. Radiol.* **2009**, *70*, 274; c) D. Pan, C. T. N. Pham, K. N. Weibaecker, M. H. Tomasson, S. A. Wickline, G. M. Lanza, *WIREs Nanomed. Nanobiotechnol.* **2016**, *8*, 85.
176. J. Gao, M. Zhu, H. Huang, Y. Liu, Z. Kang, *Inorg. Chem. Front.* **2017**, *4*, 1963.
177. a) K. Ghosal, A. Ghosh, *Mater. Sci. Eng. C Mater. Biol. Appl.* **2019**, *96*, 887; b) S. K. Misra, H.-H. Chang, P. Mukherjee, S. Tiwari, A. Ohoka, D. Pan, *Sci. Rep.* **2015**, *5*, 14986; c) P. Fathi, A. Roslind, K. Mehta, P. Moitra, K. Zhang, D. Pan, *Nanoscale* **2021**; d) A. S. Schwartz-Duval, C. J. Konopka, P. Moitra, E. A. Daza, I. Srivastava, E. V. Johnson, T. L. Kampert, S. Fayn, A.

- Haran, L. W. Dobrucki, D. Pan, *Nat. Commun.* **2020**, *11*, 4530; e) P. Moitra, D. Bhagat, R. Pratap, S. Bhattacharya, *Sci. Rep.* **2016**, *6*, 37355; f) K. Kumar, P. Moitra, M. Bashir, P. Kondaiyah, S. Bhattacharya, *Nanoscale* **2020**, *12*, 1067; g) K. O. Boakye-Yiadom, S. Kesse, Y. Opoku-Damoah, M. S. Filli, M. Aquib, M. M. B. Joelle, M. A. Farooq, R. Mavlyanova, F. Raza, R. Bavi, B. Wang, *Int. J. Pharm.* **2019**, *564*, 308; h) P. Ray, J. L. Gray, J. V. Badding, A. D. Lueking, *J. Phys. Chem. B* **2016**, *120*, 11035; i) F. Ostadhossein, D. Sar, I. Tripathi, J. Soares, E. E. Remsen, D. Pan, *ACS Appl. Mater. Interfaces* **2020**, *12*, 10183; j) S. K. Misra, A. S. Schwartz-Duval, F. Ostadhossein, E. A. Daza, Z. M. Saldivar, B. K. Sharma, D. Pan, *ACS Appl. Mater. Interfaces* **2017**, *9*, 21147; k) F. Ostadhossein, S. K. Misra, A. S. Schwartz-Duval, B. K. Sharma, D. Pan, *ACS Appl. Mater. Interfaces* **2017**, *9*, 11528; l) D. Pan, *Mol. Pharm.* **2013**, *10*, 781; m) P. Moitra, K. Kumar, P. Kondaiyah, S. Bhattacharya, *Angew. Chem., Int. Ed. Engl.* **2014**, *53*, 1113; n) S. K. Misra, P. Moitra, B. S. Chhikara, P. Kondaiyah, S. Bhattacharya, *J. Mater. Chem.* **2012**, *22*, 7985; o) P. Moitra, K. Kumar, S. Sarkar, P. Kondaiyah, W. Duan, S. Bhattacharya, *Chem. Commun.* **2017**, *53*, 8184; p) S. K. Misra, P. Moitra, P. Kondaiyah, S. Bhattacharya, *Colloids Surf. B* **2016**, *142*, 130; q) M. Kamra, P. Moitra, D. Ponnalagu, A. A. Karande, S. Bhattacharya, *ACS Appl. Mater. Interfaces* **2019**, *11*, 37442; r) S. Datta, S. K. Misra, M. L. Saha, N. Lahiri, J. Louie, D. Pan, P. J. Stang, *Proc. Natl. Acad. Sci.* **2018**, *115*, 8087; s) C. T. Pham, D. G. Thomas, J. Beiser, L. M. Mitchell, J. L. Huang, A. Senpan, G. Hu, M. Gordon, N. A. Baker, D. Pan, G. M. Lanza, D. E. Hourcade, *Nanomedicine* **2014**, *10*, 651; t) D. Pan, A. H. Schmieder, K. Wang, X. Yang, A. Senpan, G. Cui, K. Killgore, B. Kim, J. S. Allen, H. Zhang, S. D. Caruthers, B. Shen, S. A. Wickline, G. M. Lanza, *Theranostics* **2014**, *4*, 565; u) D. Soodgupta, D. Pan, G. Cui, A. Senpan, X. Yang, L. Lu, K. N. Weilbaecher, E. V. Prochownik, G. M. Lanza, M. H. Tomasson, *Mol. Cancer Ther.* **2015**, *14*, 1286; v) R. Zhang, D. Pan, X. Cai, X. Yang, A. Senpan, J. S. Allen, G. M. Lanza, L. V. Wang, *Theranostics* **2015**, *5*, 124; w) A. Das, I. Haque, P. Ray, A. Ghosh, D. Dutta, M. Quadir, A. De, S. Gunewardena, I. Chatterjee, S. Banerjee, S. Weir, S. K. Banerjee, *Pharmacol. Res. Perspect.* **2021**, *9*, e00753.
178. S. K. Misra, P. Mukherjee, H. H. Chang, S. Tiwari, M. Gryka, R. Bhargava, D. Pan, *Sci. Rep.* **2016**, *6*, 29299.
179. I. Srivastava, S. K. Misra, F. Ostadhossein, E. Daza, J. Singh, D. Pan, *Nano Res.* **2017**, *10*, 3269.
180. T. Kong, L. Hao, Y. Wei, X. Cai, B. Zhu, *Cell Prolif.* **2018**, *51*, e12488.
181. S. Beack, W. H. Kong, H. S. Jung, I. H. Do, S. Han, H. Kim, K. S. Kim, S. H. Yun, S. K. Hahn, *Acta Biomater.* **2015**, *26*, 295.
182. J. Kim, J. Park, H. Kim, K. Singha, W. J. Kim, *Biomaterials* **2013**, *34*, 7168.
183. H. Wang, J. Shen, Y. Li, Z. Wei, G. Cao, Z. Gai, K. Hong, P. Banerjee, S. Zhou, *Biomater. Sci.* **2014**, *2*, 915.
184. W. Wang, Y.-C. Lu, H. Huang, J.-J. Feng, J.-R. Chen, A.-J. Wang, *Analyst* **2014**, *139*, 1692.
185. T. Feng, X. Ai, G. An, P. Yang, Y. Zhao, *ACS Nano* **2016**, *10*, 4410.
186. P. Huang, J. Lin, X. Wang, Z. Wang, C. Zhang, M. He, K. Wang, F. Chen, Z. Li, G. Shen, D. Cui, X. Chen, *Adv. Mater.* **2012**, *24*, 5104.
187. L. Zhou, Z. Li, Z. Liu, J. Ren, X. Qu, *Langmuir* **2013**, *29*, 6396.
188. N. Gao, W. Yang, H. Nie, Y. Gong, J. Jing, L. Gao, X. Zhang, *Biosens. Bioelectron.* **2017**, *96*, 300.
189. S. Pandey, M. Thakur, A. Mewada, D. Anjarlekar, N. Mishra, M. Sharon, *J. Mater. Chem. B* **2013**, *1*, 4972.
190. S. K. Misra, A. Ohoka, N. J. Kolmodin, D. Pan, *Mol. Pharm.* **2015**, *12*, 375.
191. S. Li, D. Amat, Z. Peng, S. Vanni, S. Raskin, G. De Angulo, A. M. Othman, R. M. Graham, R. M. Leblanc, *Nanoscale* **2016**, *8*, 16662.
192. X. T. Zheng, A. Ananthanarayanan, K. Q. Luo, P. Chen, *Small* **2015**, *11*, 1620.
193. Y. Yan, J. Gong, J. Chen, Z. Zeng, W. Huang, K. Pu, J. Liu, P. Chen, *Adv. Mater.* **2019**, *31*, 1808283.
194. a) C. Wu, C. Wang, T. Han, X. Zhou, S. Guo, J. Zhang, *Adv. Healthcare Mater.* **2013**, *2*, 1613; b) N. R. Ko, M. Nafiujjaman, J. S. Lee, H. N. Lim, Y. k. Lee, I. K. Kwon, *RSC Adv.* **2017**, *7*, 11420; c) S. K. Misra, A. De, D. Pan, *Mol. Cancer Ther.* **2018**, *17*, 119.
195. A. Alaghamandfard, O. Sedighi, N. Tabatabaei Rezaei, A. A. Abedini, A. Malek Khachaturian, M. S. Toprak, A. Seifalian, *Mater. Sci. Eng. C*, **2021**, *120*, 111756.
196. X. Yuan, Z. Liu, Z. Guo, Y. Ji, M. Jin, X. Wang, *Nanoscale Res. Lett.* **2014**, *9*, 108.
197. Y. Chong, Y. Ma, H. Shen, X. Tu, X. Zhou, J. Xu, J. Dai, S. Fan, Z. Zhang, *Biomaterials* **2014**, *35*, 5041.
198. A. Chandra, S. Deshpande, D. B. Shinde, V. K. Pillai, N. Singh, *ACS Macro Lett.* **2014**, *3*, 1064.
199. C. Hoskins, A. Cuschieri, L. Wang, *J. Nanobiotechnol.* **2012**, *10*, 15.
200. G. Zhang, Z. Yang, W. Lu, R. Zhang, Q. Huang, M. Tian, L. Li, D. Liang, C. Li, *Biomaterials* **2009**, *30*, 1928.
201. N. Licciardello, S. Hunoldt, R. Bergmann, G. Singh, C. Mamat, A. Faramus, J. L. Z. Ddungu, S. Silvestrini, M. Maggini, L. De Cola, H. Stephan, *Nanoscale* **2018**, *10*, 9880.
202. L. Guerrini, R. A. Alvarez-Puebla, N. Pazos-Perez, *Materials* **2018**, *11*.
203. T. Malina, K. Poláková, J. Skopalík, V. Milotová, K. Holá, M. Havrdová, K. B. Tománková, V. Čmiel, L. Šefc, R. Zbořil, *Carbon* **2019**, *152*, 434.
204. J. Wang, G. Liu, K. C. Leung, R. Loffroy, P. X. Lu, Y. X. Wang, *Curr. Pharm. Des.* **2015**, *21*, 5401.

## AUTHOR BIOGRAPHIES



**Dr. Priyanka Ray** received her Ph.D. in nanochemistry from Université Paris XI-CNRS, Paris, France, where she worked on the synthesis and characterization of calixarenes and metal nanoparticles using gamma irradiation for bactericidal applications. She then worked under the CoBRE center at NDSU in Fargo, ND, on developing polymeric nanocarriers for

targeted drug delivery to treat pancreatic and breast cancer. Currently, she is working as a postdoctoral research associate in Prof. Dipanjan Pan's laboratory at the University of Maryland, Baltimore. Her research interests include drug delivery for cancer therapy and the fabrication of nanomaterials for biomedical applications.



**Dr. Parikshit Moitra** is currently working as a research associate (junior faculty) at the University of Maryland Baltimore (UMB) under the supervision of Prof. Dipanjan Pan. He has demonstrated research expertise in chemical biology, supramolecular chemistry, and bioanalyte sensors. During his postdoctoral stint, he worked with Prof. Pan at UMB School of Medicine. He received his Ph.D. degree from the Indian Institute of Science, Bangalore, India.



**Prof. Dr. Dipanjan Pan** is a full professor in the Department of Diagnostic Radiology and Nuclear Medicine, Pediatrics at the University of Maryland Baltimore and Chemical, Biochemical and Environmental Engineering at the University of Maryland Baltimore County. Prof. Pan is a recognized expert in nanomedicine with particular expertise in molecular imaging, drug delivery, biosensors, and analytical measures.

**How to cite this article:** Ray P, Moitra P, Pan D. Emerging theranostic applications of carbon dots and its variants. *VIEW*. 2021;20200089. <https://doi.org/10.1002/VIW.20200089>